US 20230304193A1

(19) **United States**

(12) **Patent Application Publication**

Franklin et al.

(10) **Pub. No.: US 2023/0304193 A1**

(43) **Pub. Date: Sep. 28, 2023**

(54) **DRY-JET WET-SPINNING OF MULTIFUNCTIONAL CARBON FIBERS**

(71) Applicants: **Rahul Franklin**, West Lafayette, IN (US); **Weiheng Xu**, Chandler, AZ (US); **Dharneedar Ravichandran**, Tempe, AZ (US); **Sayli Jambhulkar**, Gilbert, AZ (US); **Yuxiang Zhu**, Gilbert, AZ (US); **Kenan Song**, Gilbert, AZ (US)

(72) Inventors: **Rahul Franklin**, West Lafayette, IN (US); **Weiheng Xu**, Chandler, AZ (US); **Dharneedar Ravichandran**, Tempe, AZ (US); **Sayli Jambhulkar**, Gilbert, AZ (US); **Yuxiang Zhu**, Gilbert, AZ (US); **Kenan Song**, Gilbert, AZ (US)

(21) Appl. No.: **18/073,975**

(22) Filed: **Dec. 2, 2022**

Related U.S. Application Data

(60) Provisional application No. 63/285,306, filed on Dec. 2, 2021.

Publication Classification

(51) **Int. Cl.**

D01F 8/18	(2006.01)
D01F 8/08	(2006.01)
D01F 11/00	(2006.01)
D01D 5/06	(2006.01)
D01D 5/34	(2006.01)

(52) **U.S. Cl.**

CPC ... ***D01F 8/18*** (2013.01); ***D01D 5/06*** (2013.01); ***D01D 5/34*** (2013.01); ***D01F 8/08*** (2013.01); ***D01F 11/00*** (2013.01)

(57) **ABSTRACT**

A carbonized coaxial composite fiber includes an inner layer including carbonized polyacrylonitrile, a middle layer surrounding the inner layer and including carbonized graphene nanomaterials, and an exterior layer surrounding the middle layer including carbonized polyacrylonitrile. The carbonized graphene nanomaterials are aligned along a length of the coaxial composite fiber.

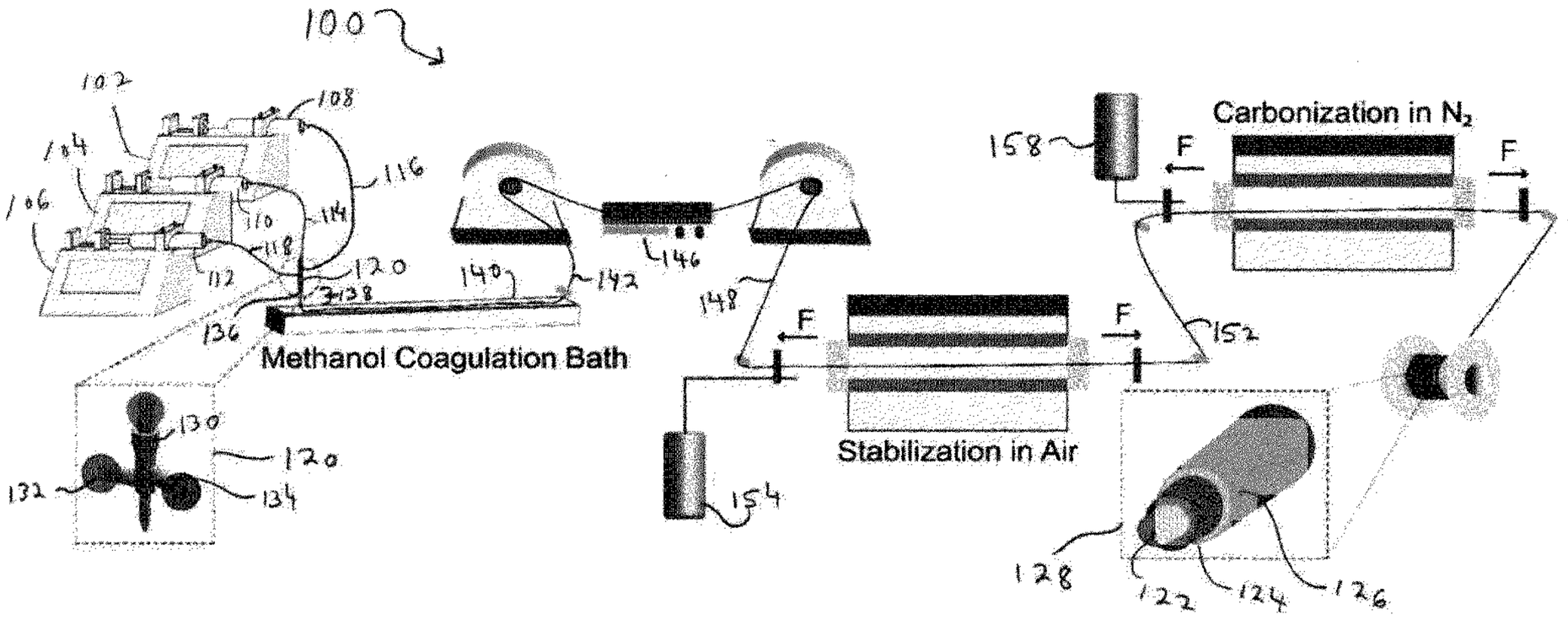

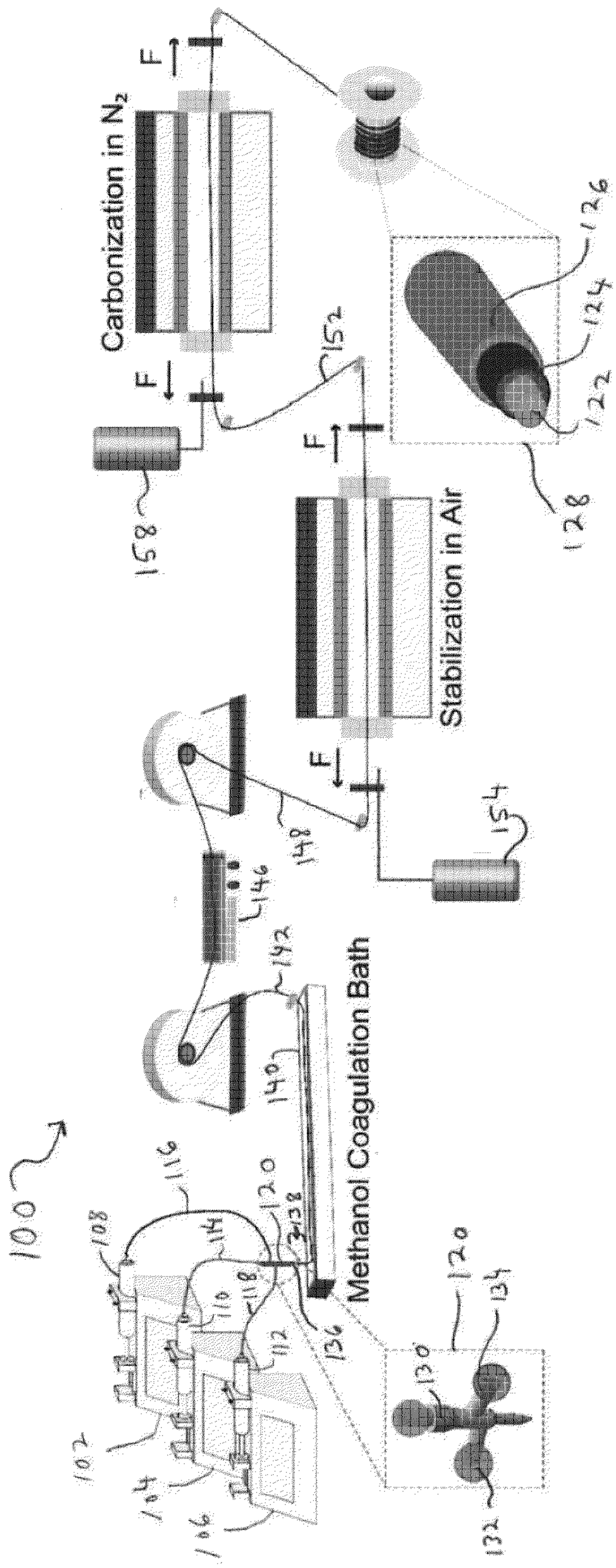
100
102
104
106
108
110
112
114
116
118
120
122
124
126
128
130
132
134
136
138
140
142
144
146
148
151
152
154
F
Carbonization in N_2
Stabilization in Air
Methanol Coagulation Bath

FIG. 1

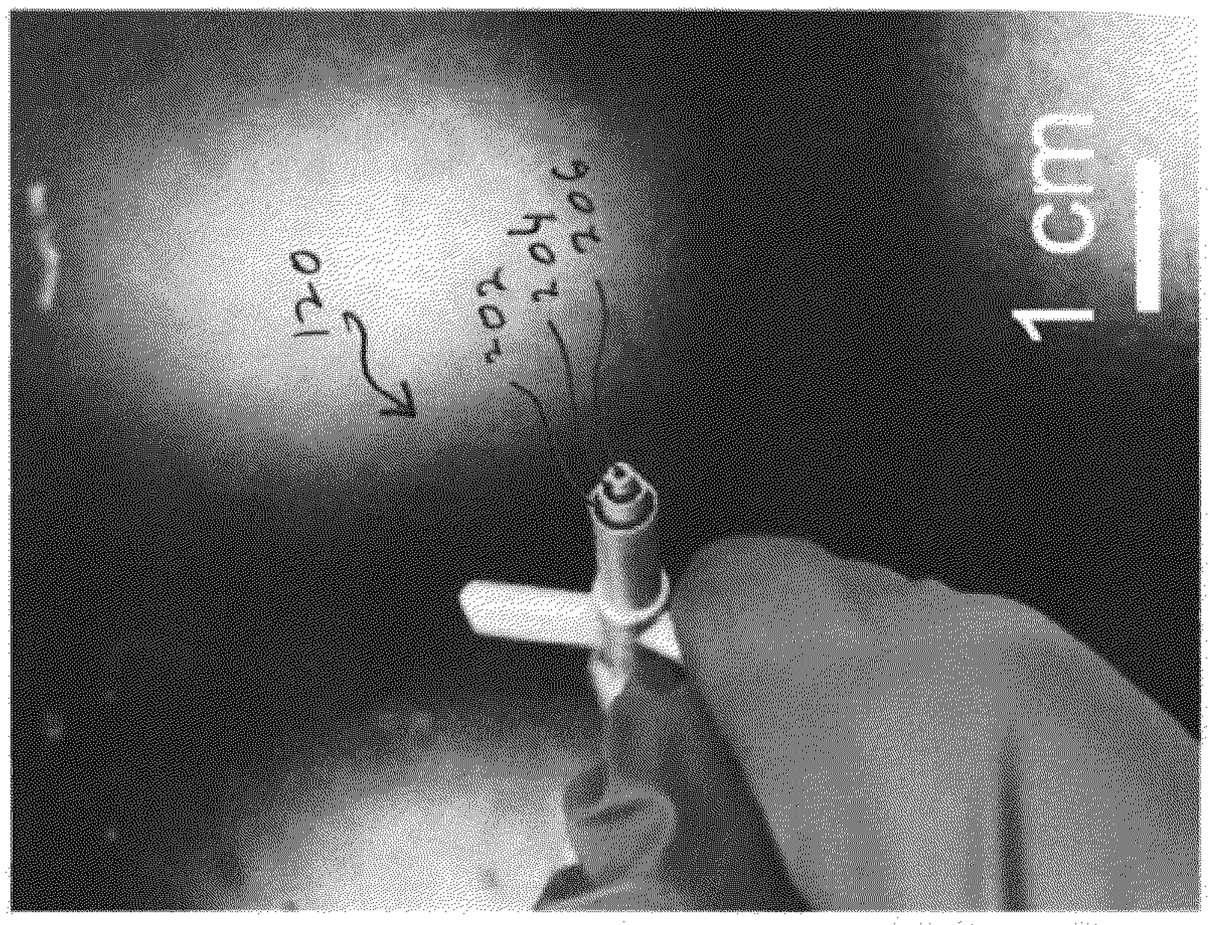

FIG. 2B

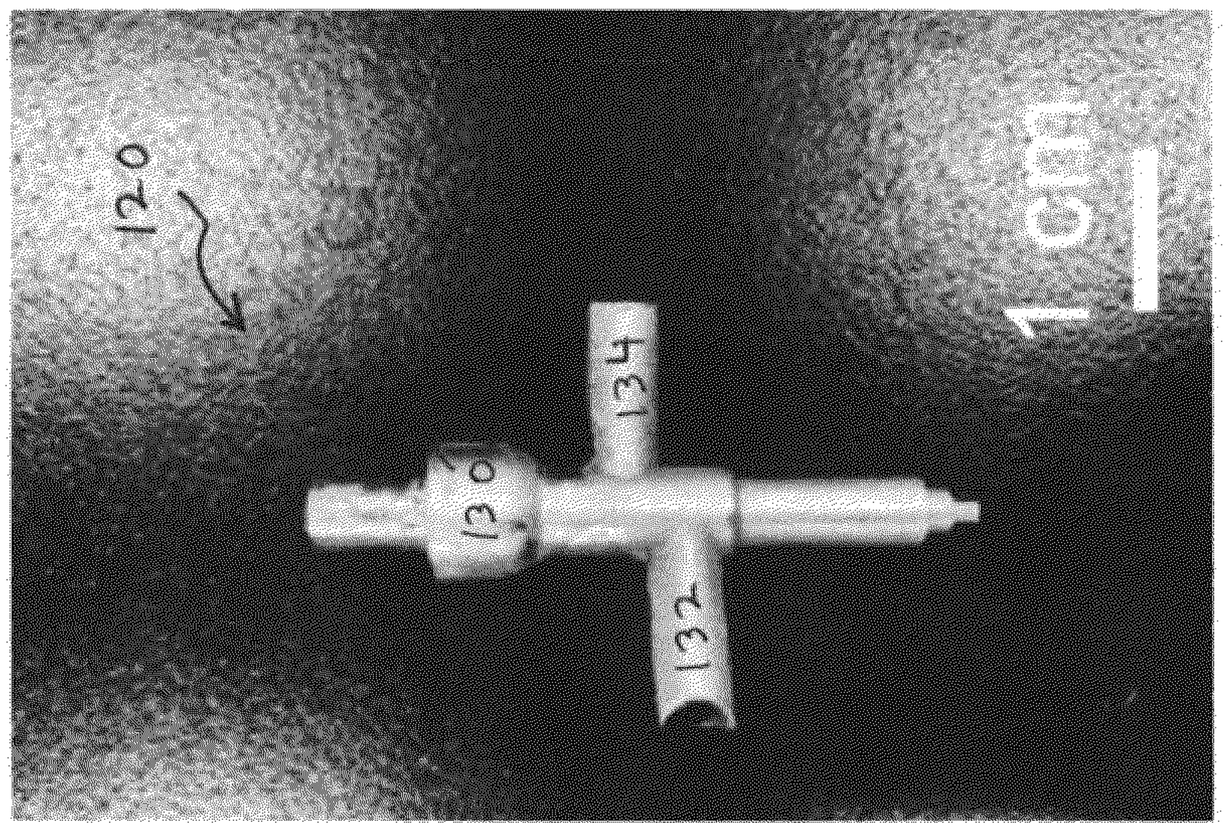

FIG. 2A

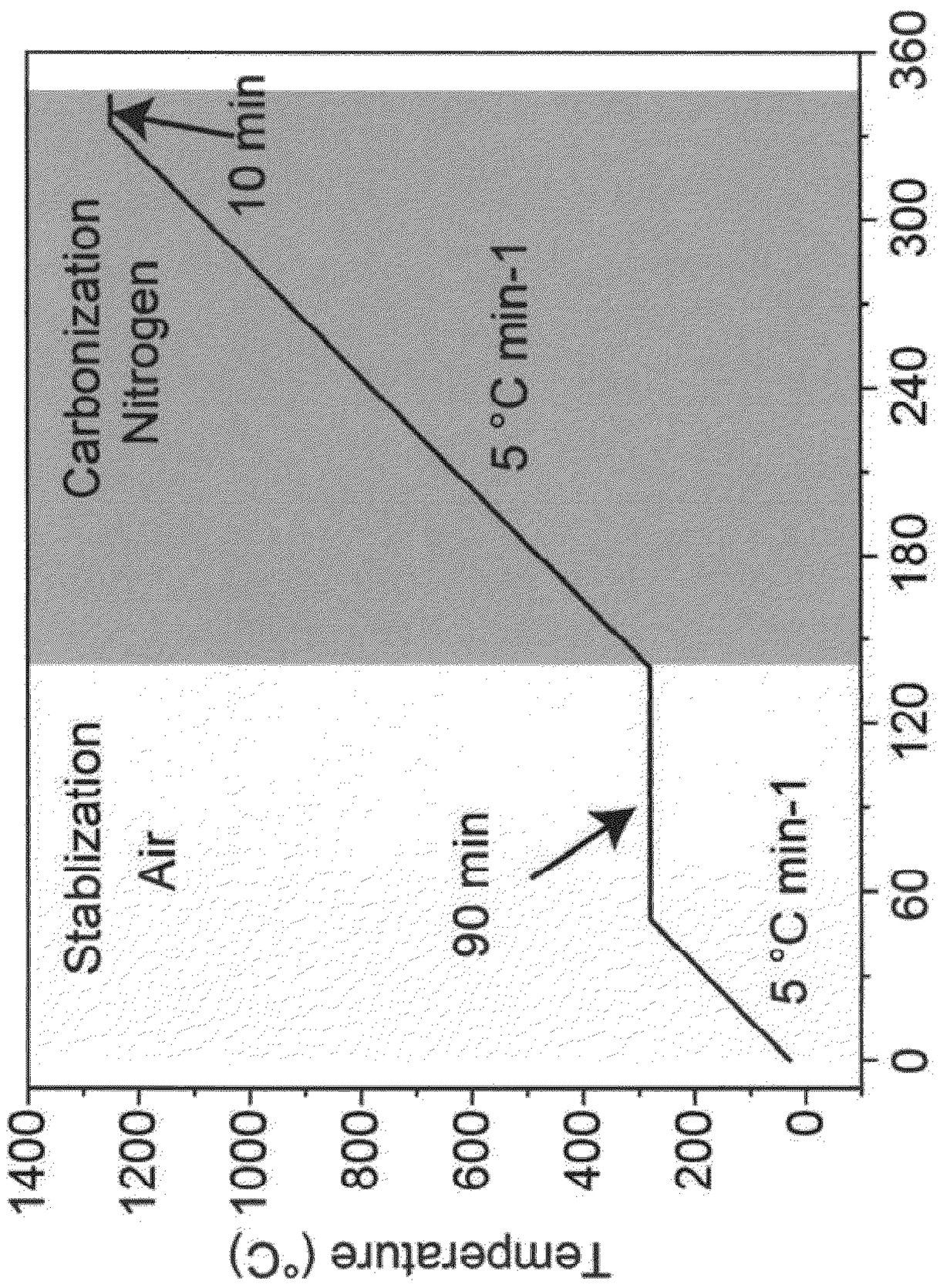
Stablization
Air
90 min
5 °C min-1
Carbonization
Nitrogen
10 min
5 °C min-1
0
60
120
180
240
300
360
Time (minutes)
1400
1200
1000
800
600
400
200
0
Temperature (°C)

FIG. 3

FIG. 4D

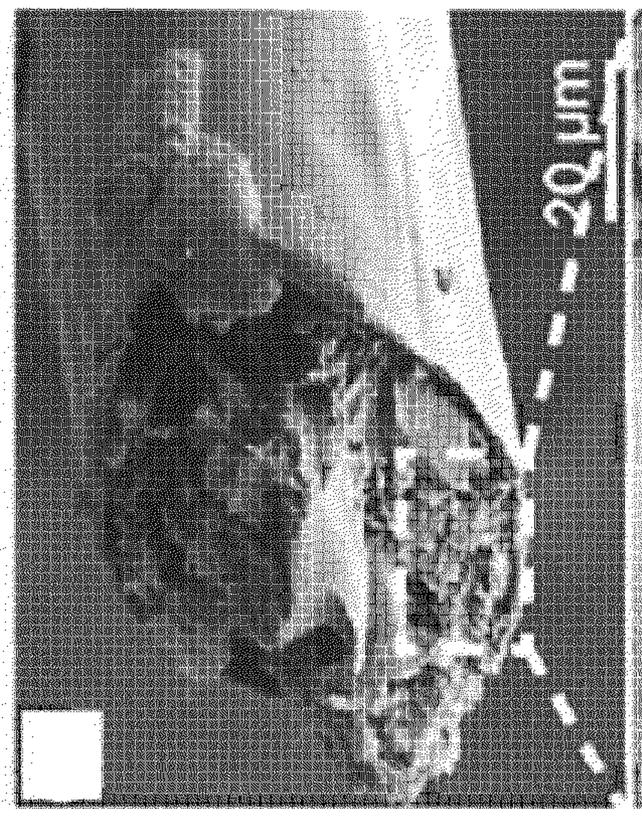

FIG. 4E

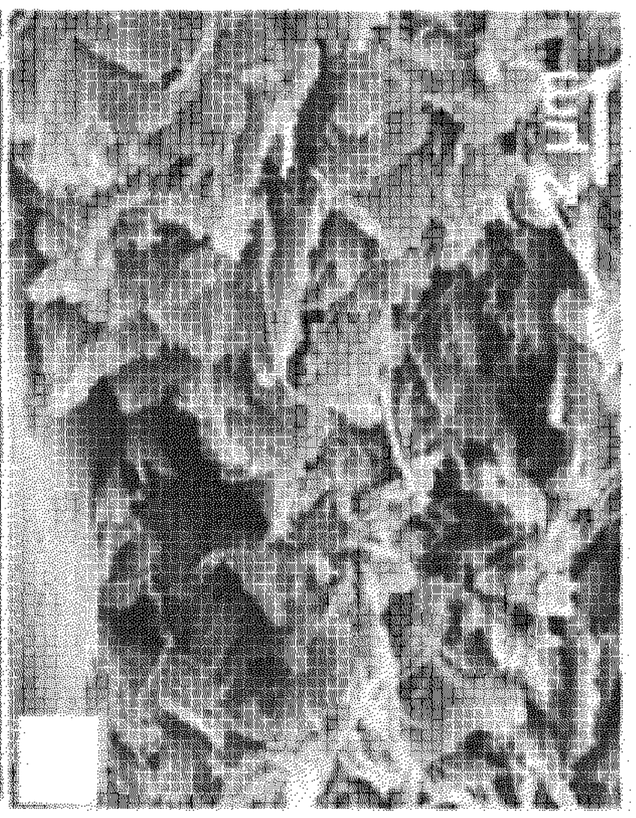

FIG. 4F

FIG. 4A

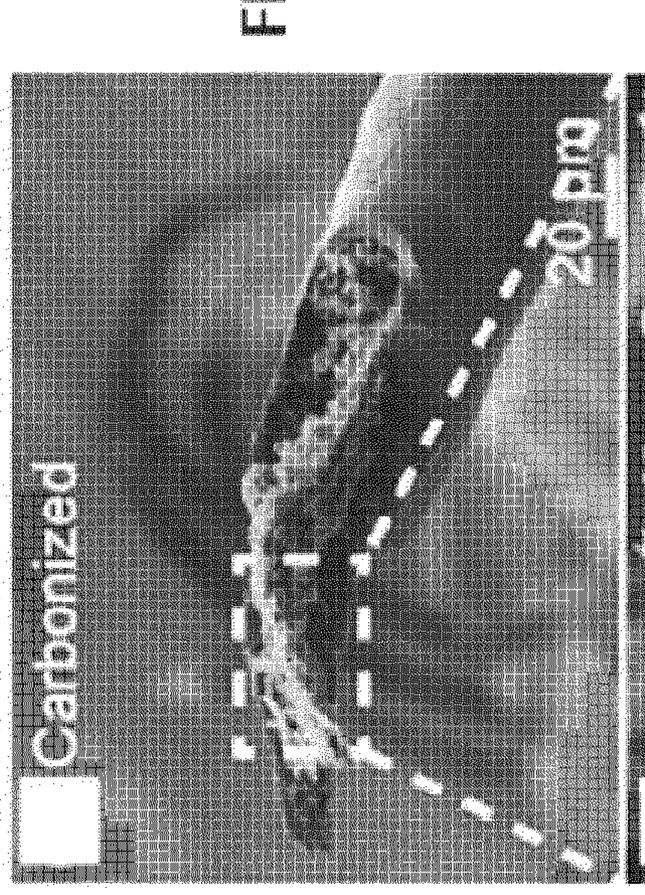

FIG. 4B

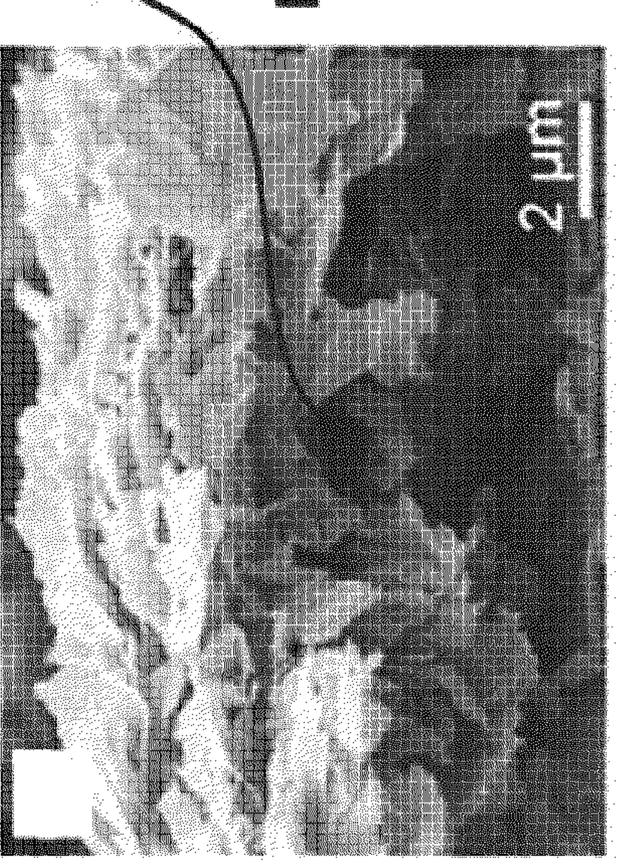

FIG. 4C

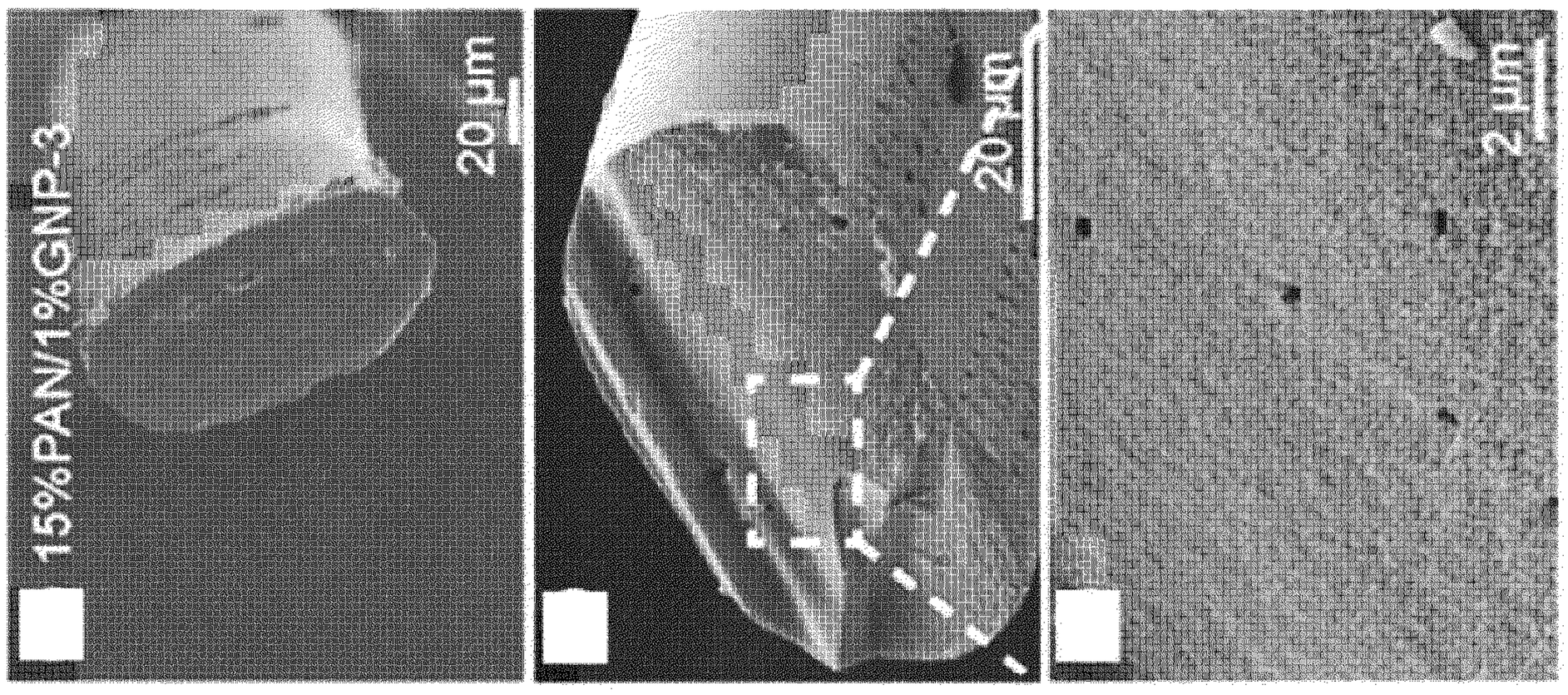

FIG. 4J FIG. 4K FIG. 4L

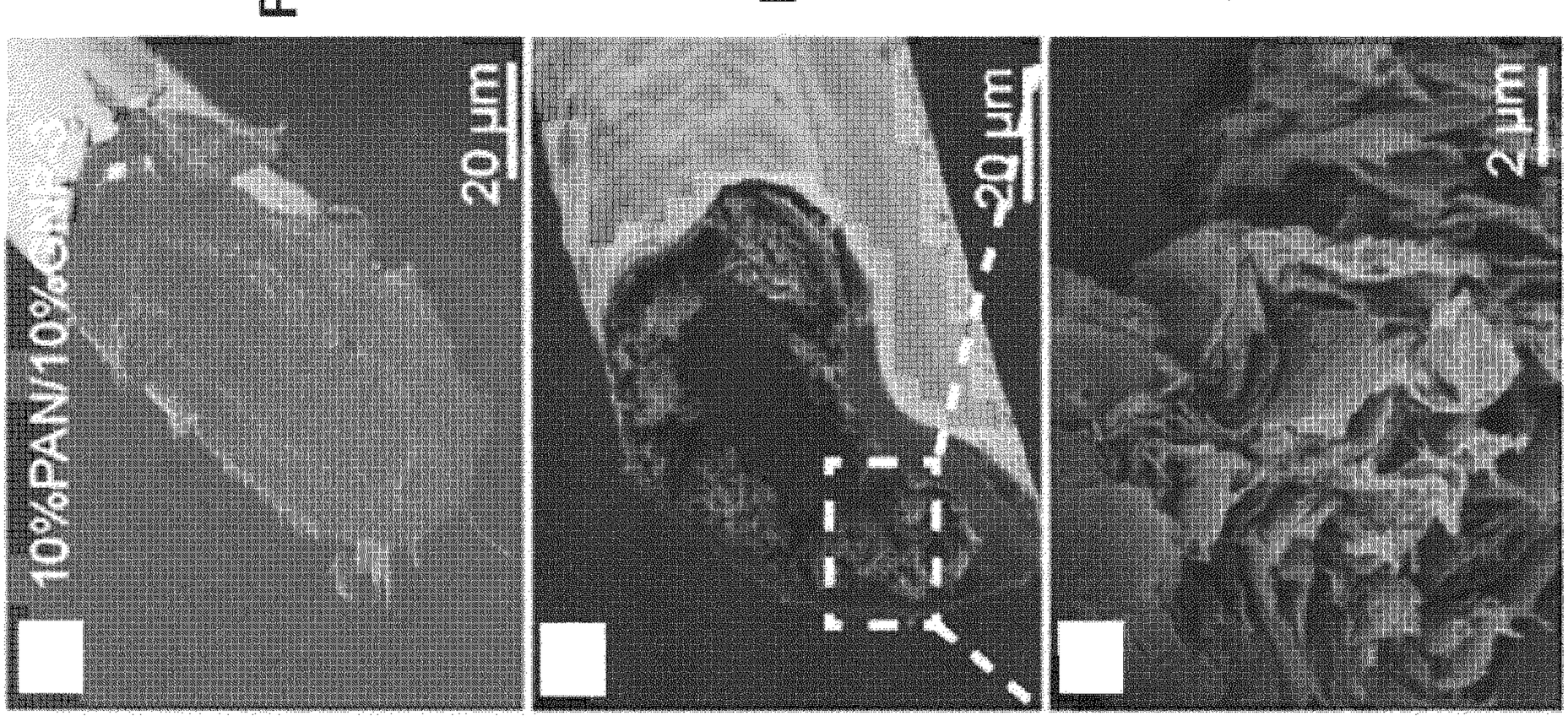

FIG. 4G FIG. 4H FIG. 4I

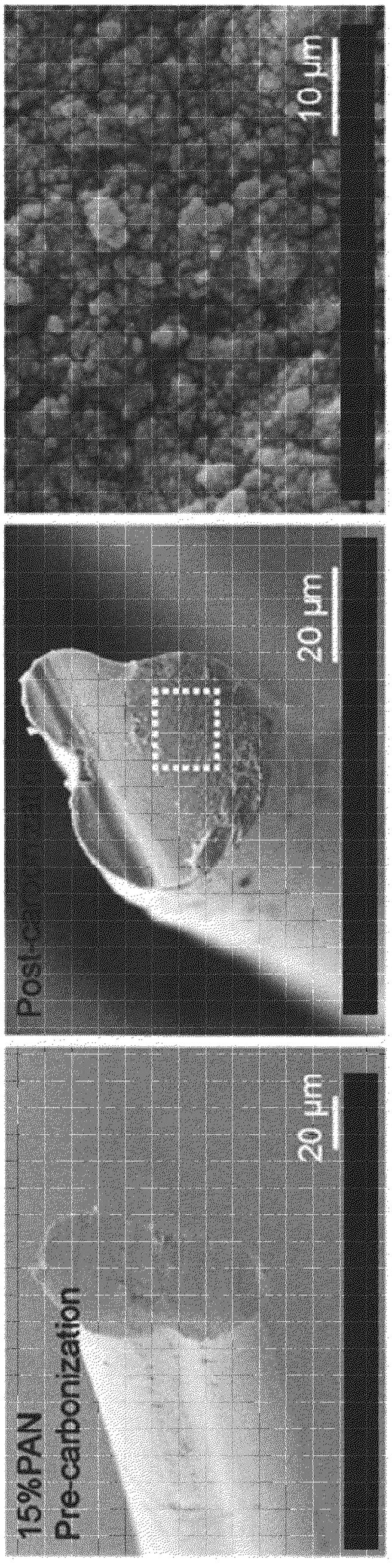

FIG. 5A

FIG. 5B

FIG. 5C

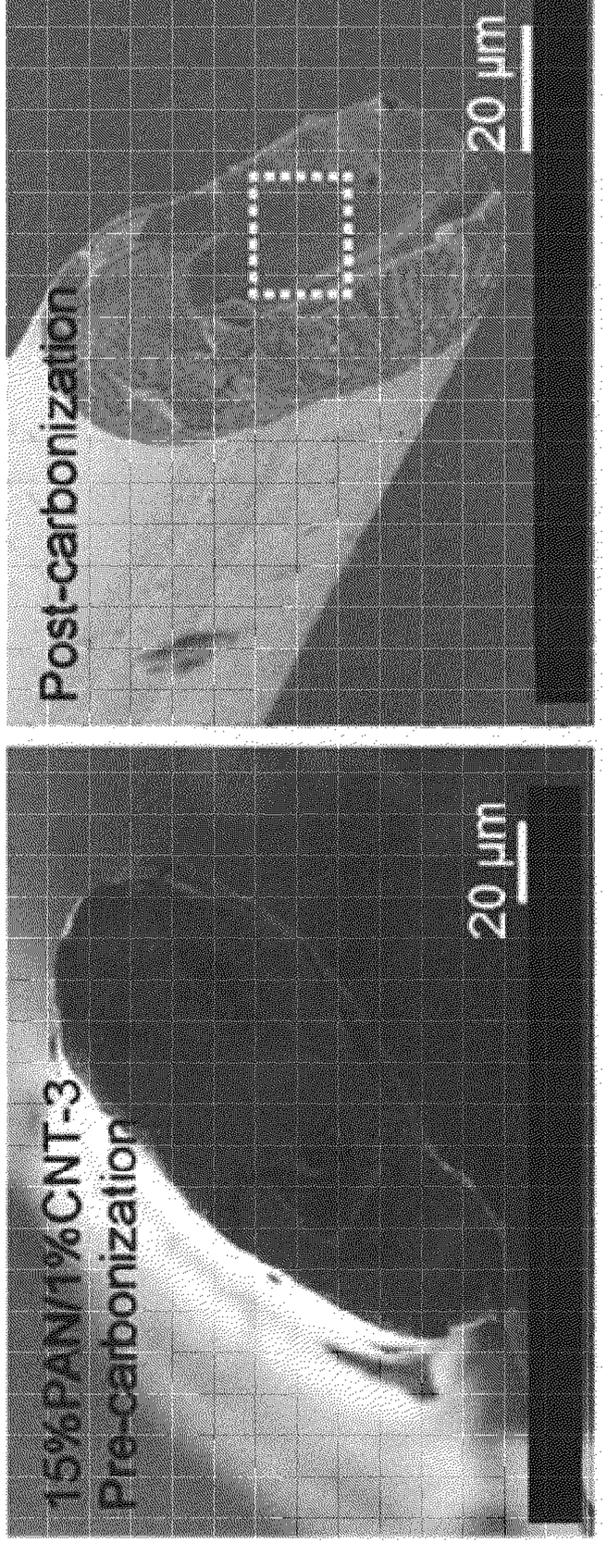

FIG. 5D

FIG. 5E

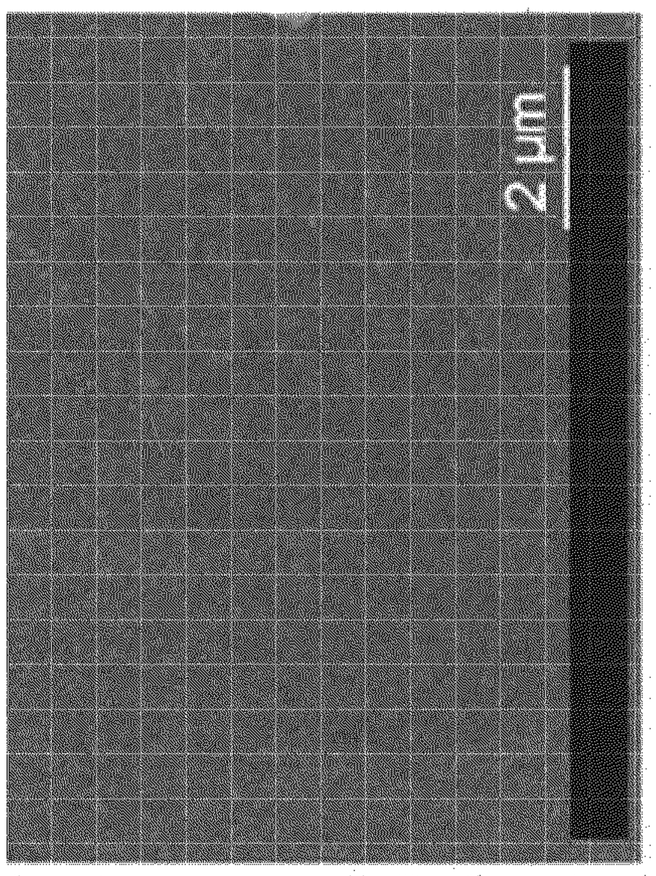

FIG. 5F

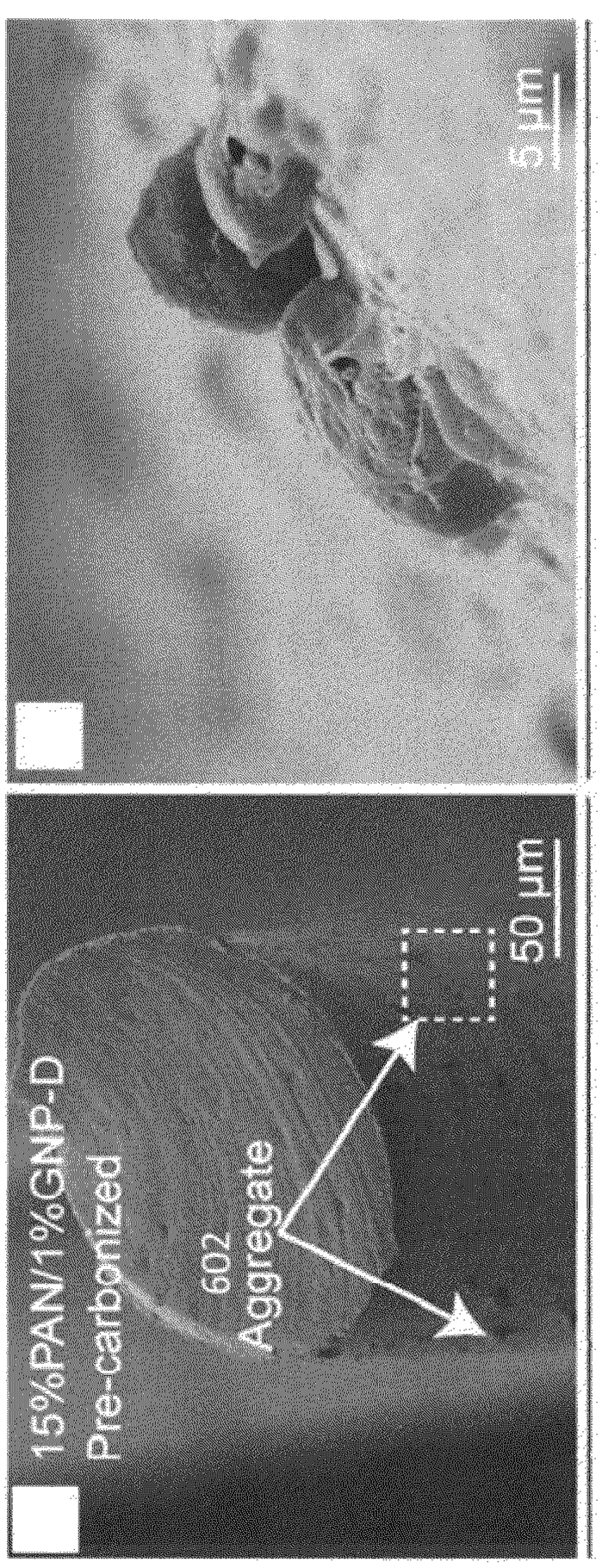

FIG. 6A

FIG. 6B

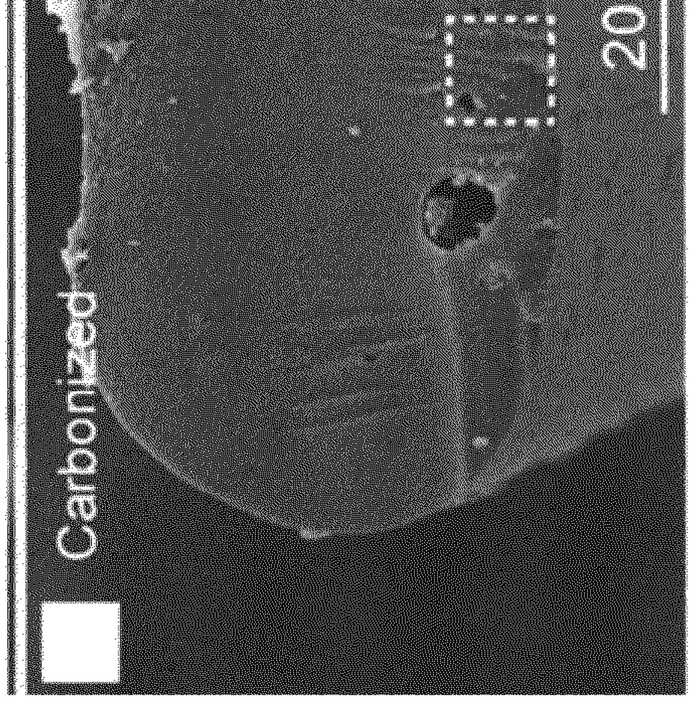

FIG. 6C

FIG. 6D

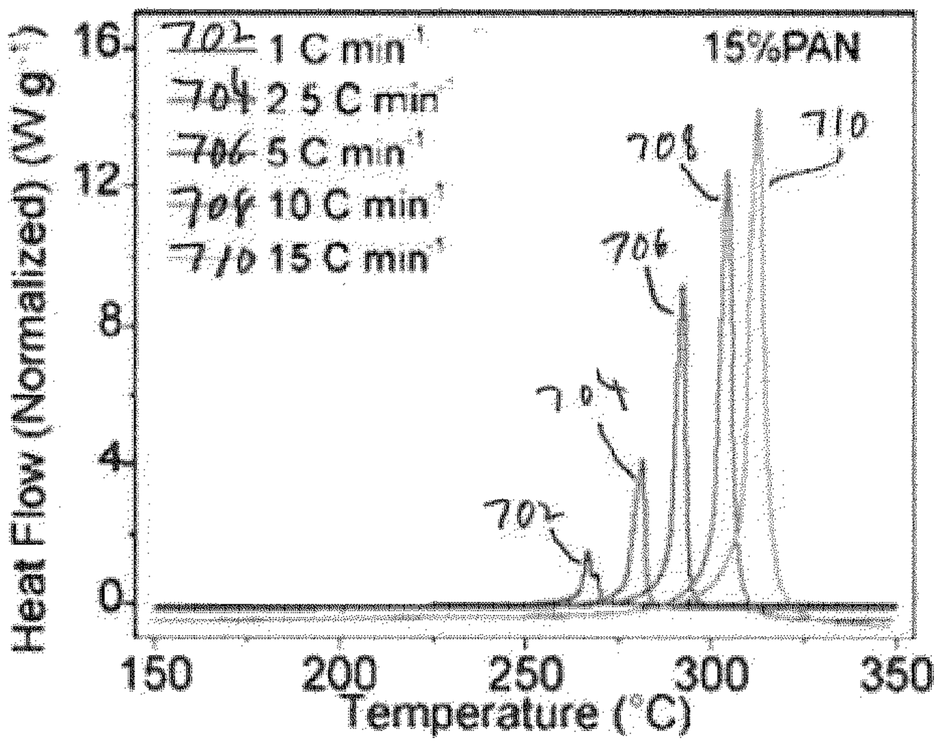

FIG. 7A

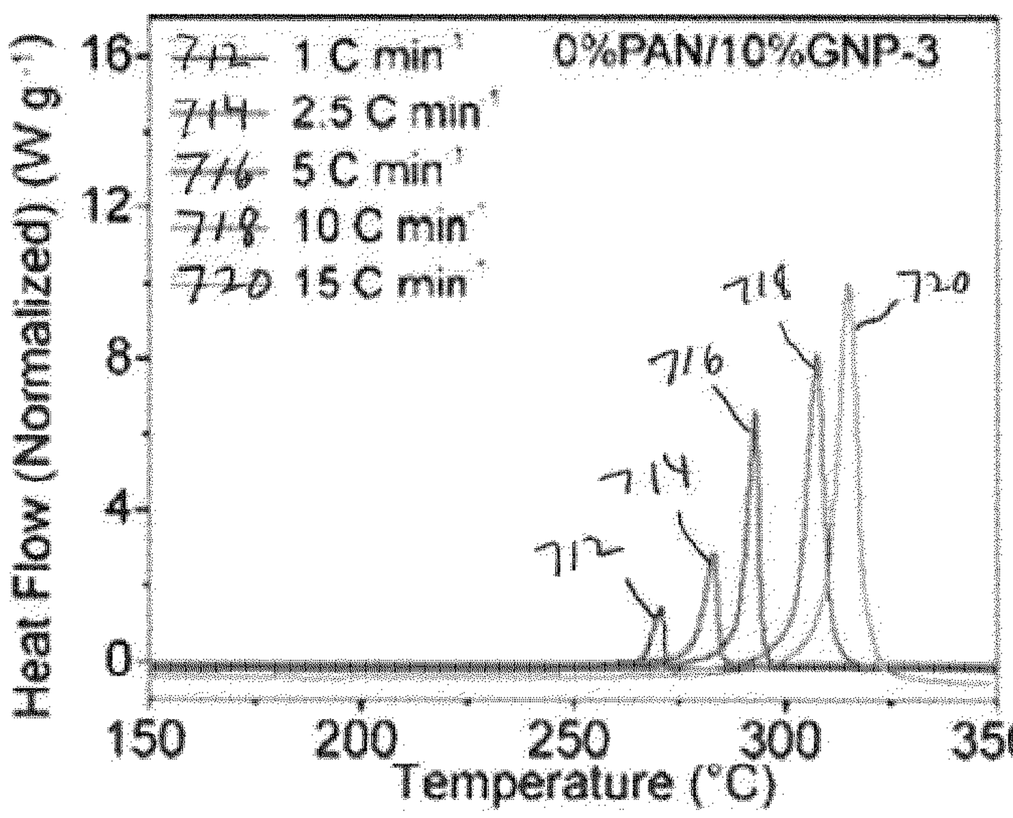

FIG. 7B

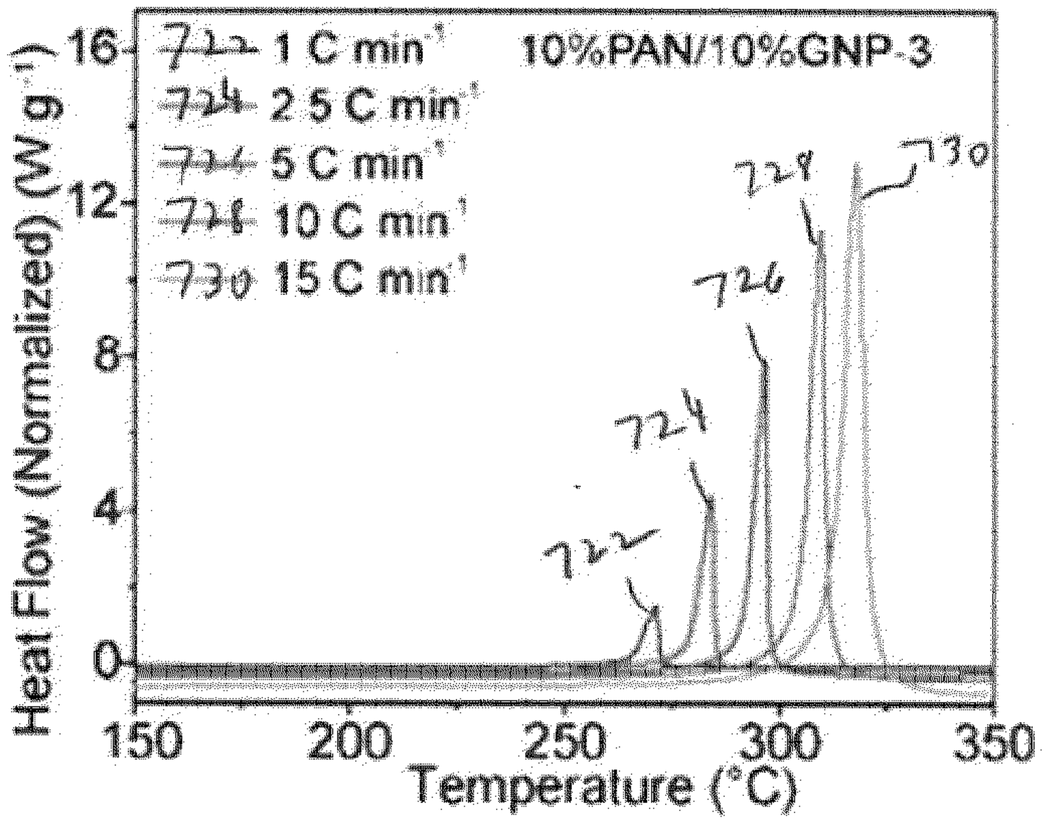

FIG. 7C

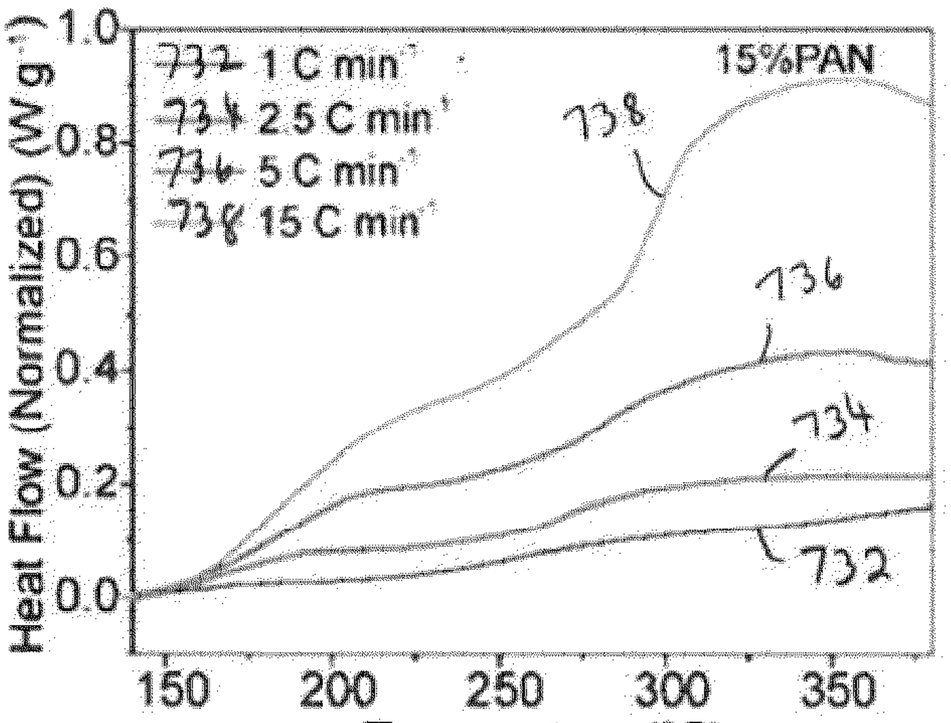

FIG. 7D

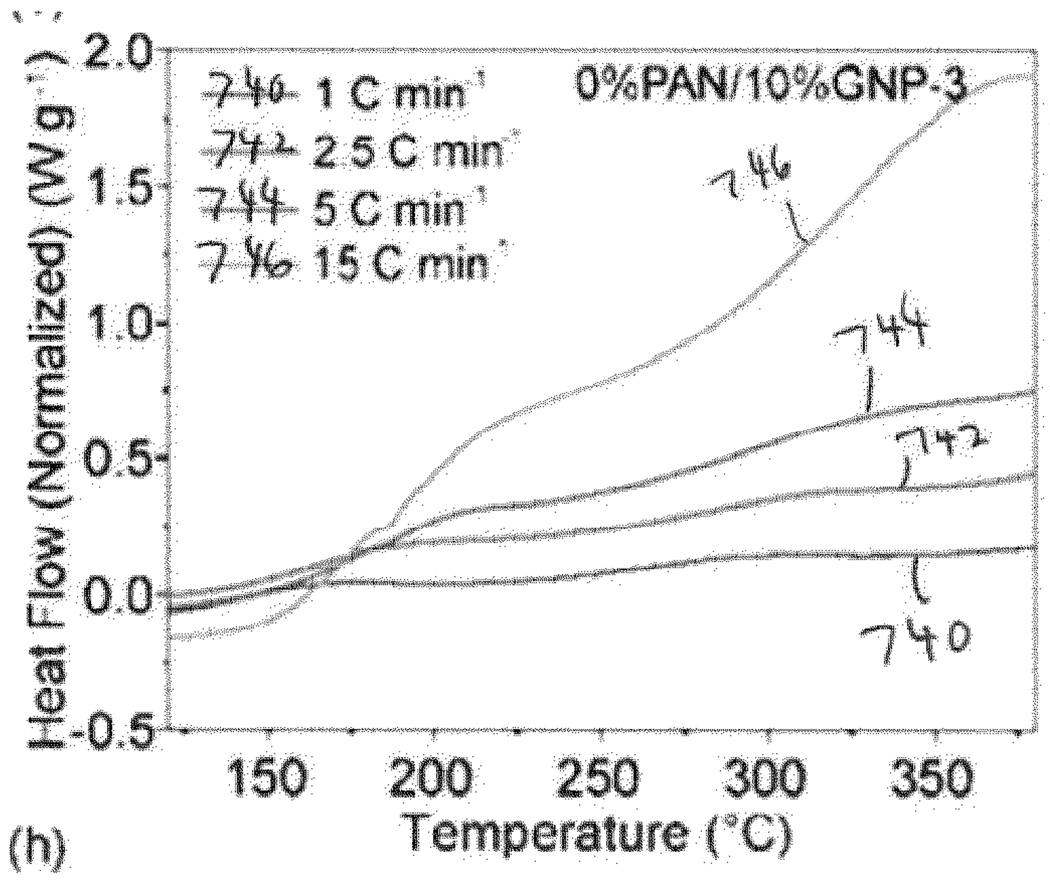

FIG. 7E

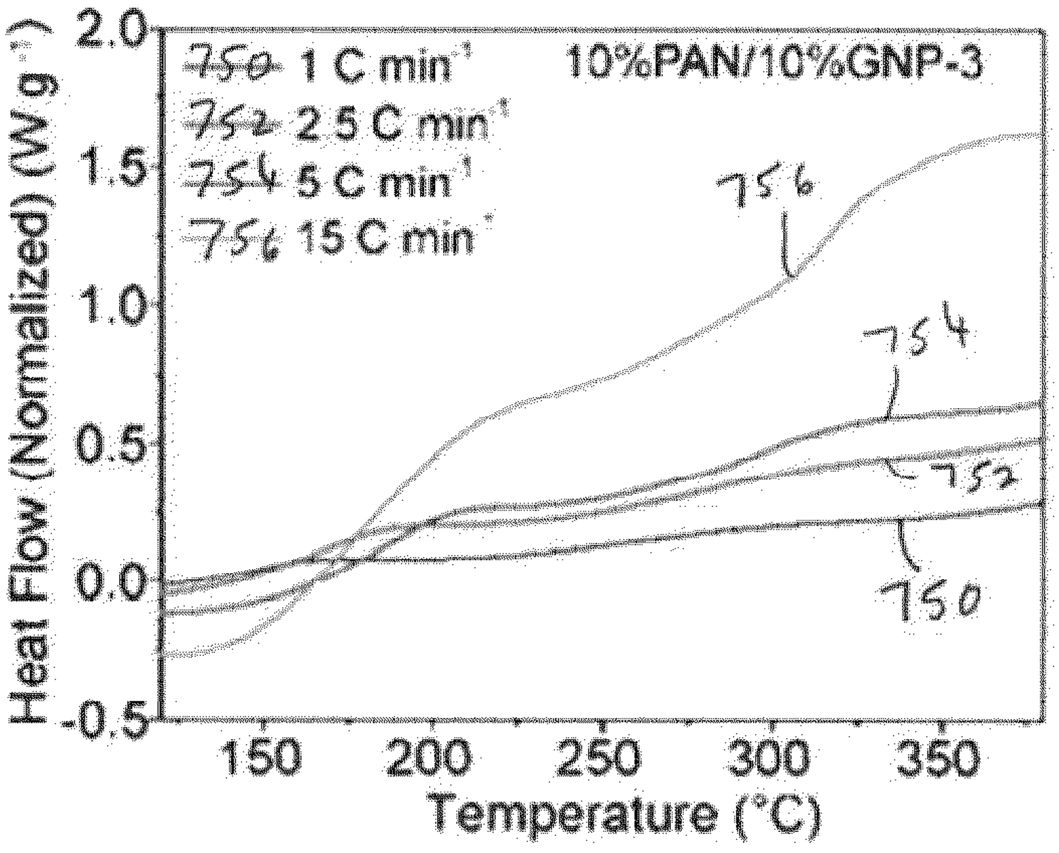

FIG. 7F

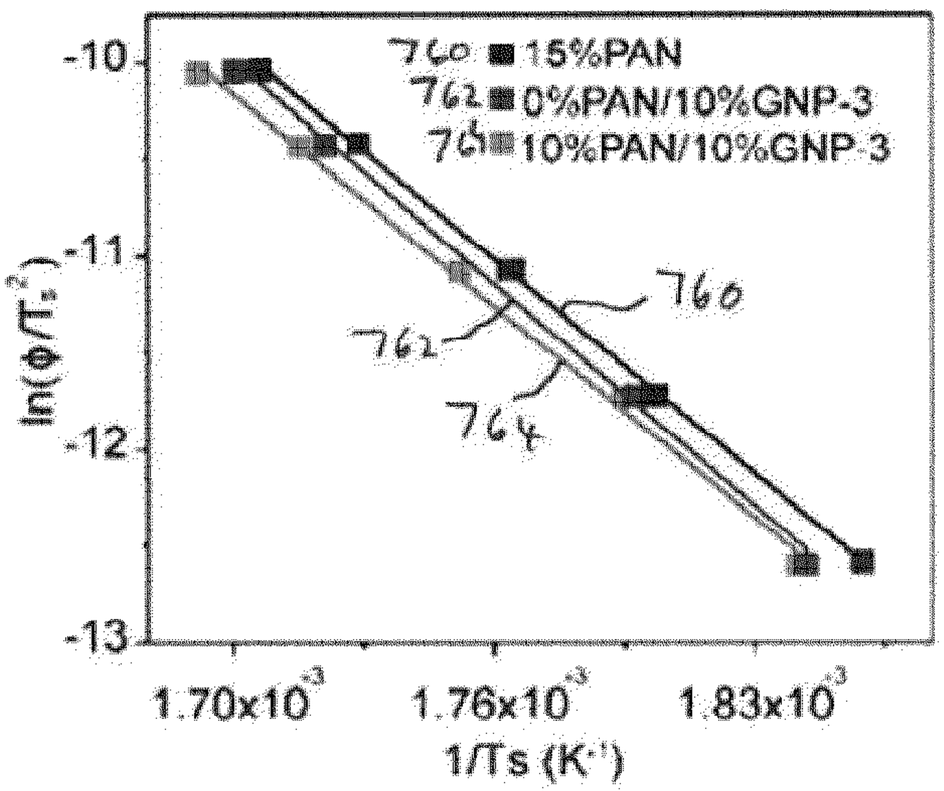

FIG. 7G

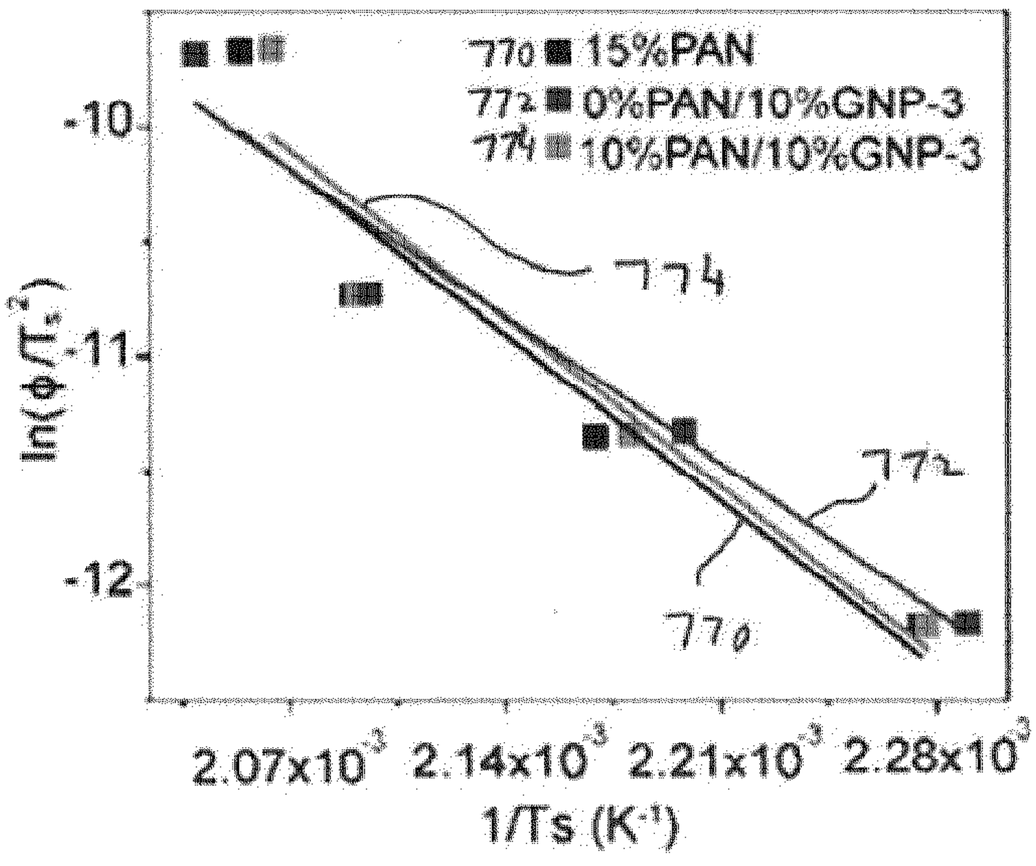

FIG. 7H

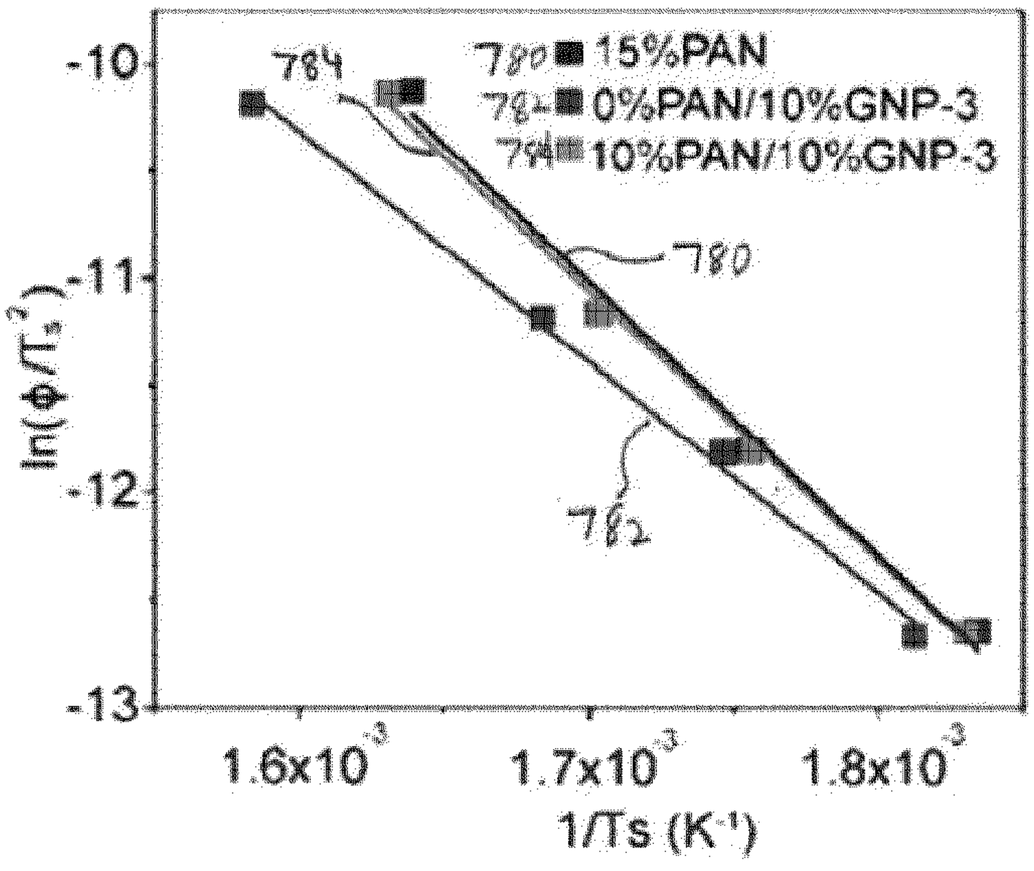

FIG. 7I

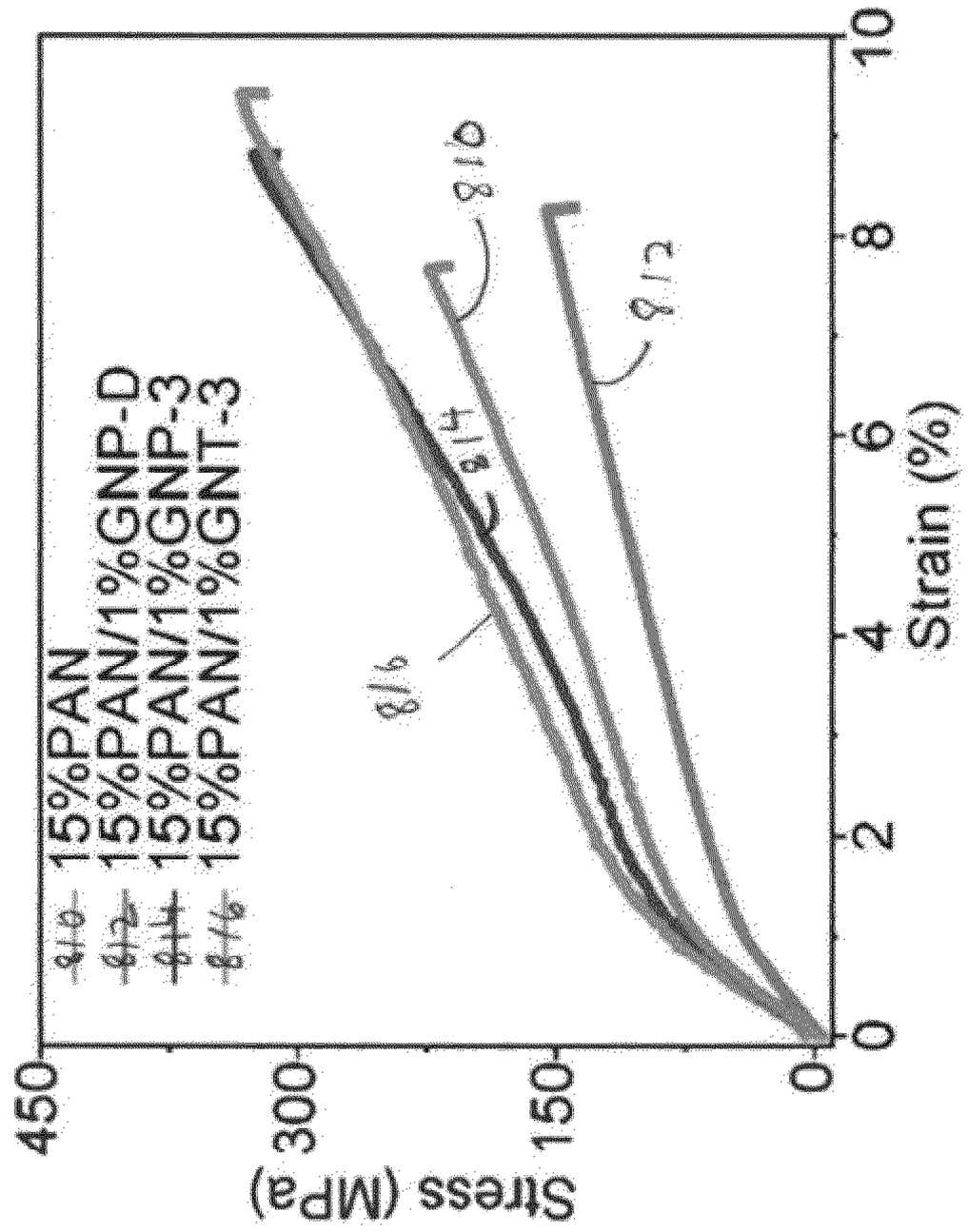
15%PAN/1%GNP-D
15%PAN/1%GNP-3
15%PAN/1%GNT-3
Stress (MPa)
Strain (%)
0
2
4
6
8
10
150
300
450

FIG. 8B

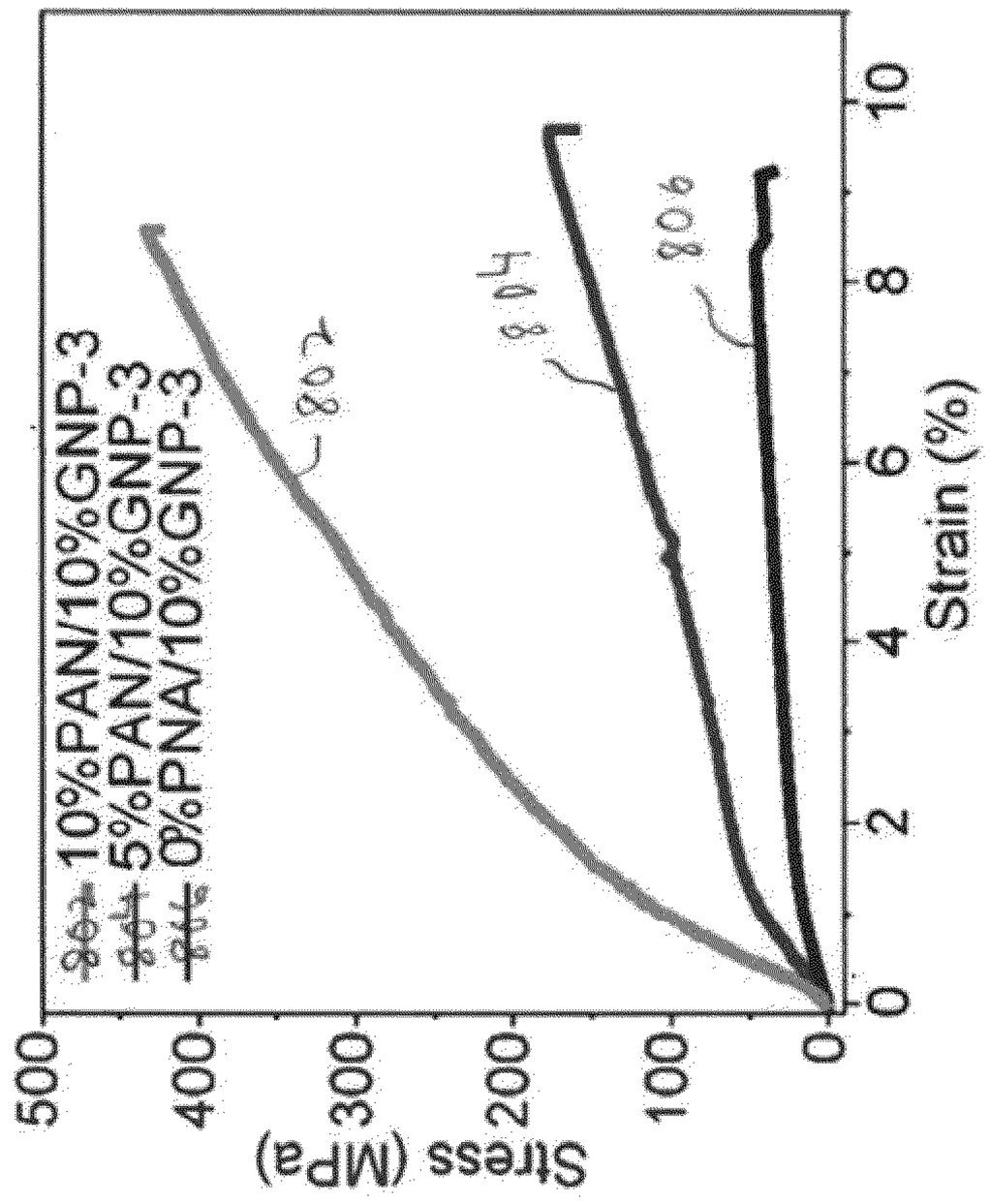
10%PAN/10%GNP-3
5%PAN/10%GNP-3
0%PNA/10%GNP-3
Stress (MPa)
Strain (%)
0
2
4
6
8
10
100
200
300
400
500

FIG. 8A

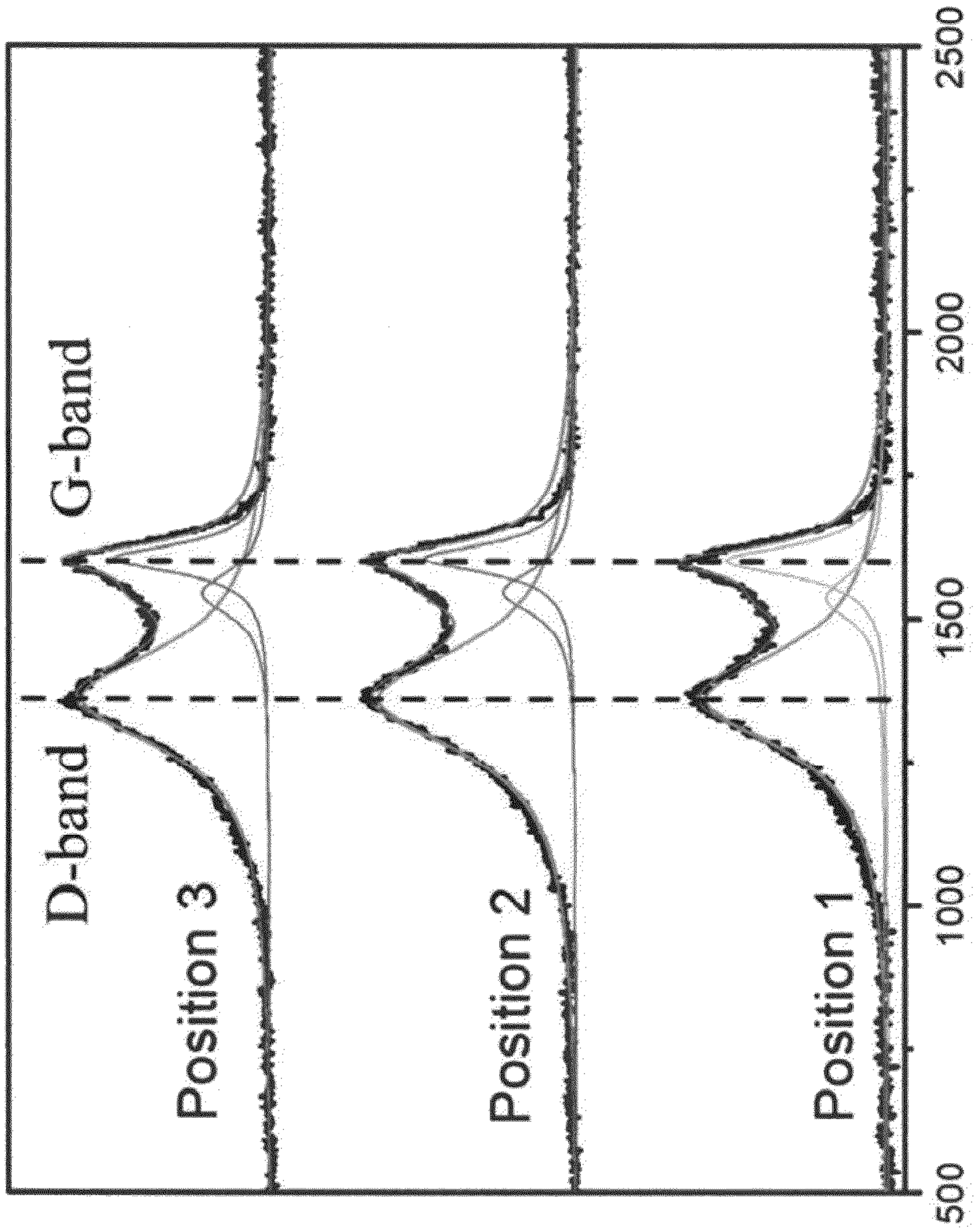
D-band
G-band
Position 3
Position 2
Position 1
2500
2000
1500
1000
500
Raman Shift (cm-1)
Intensity (a.u.)

FIG. 9

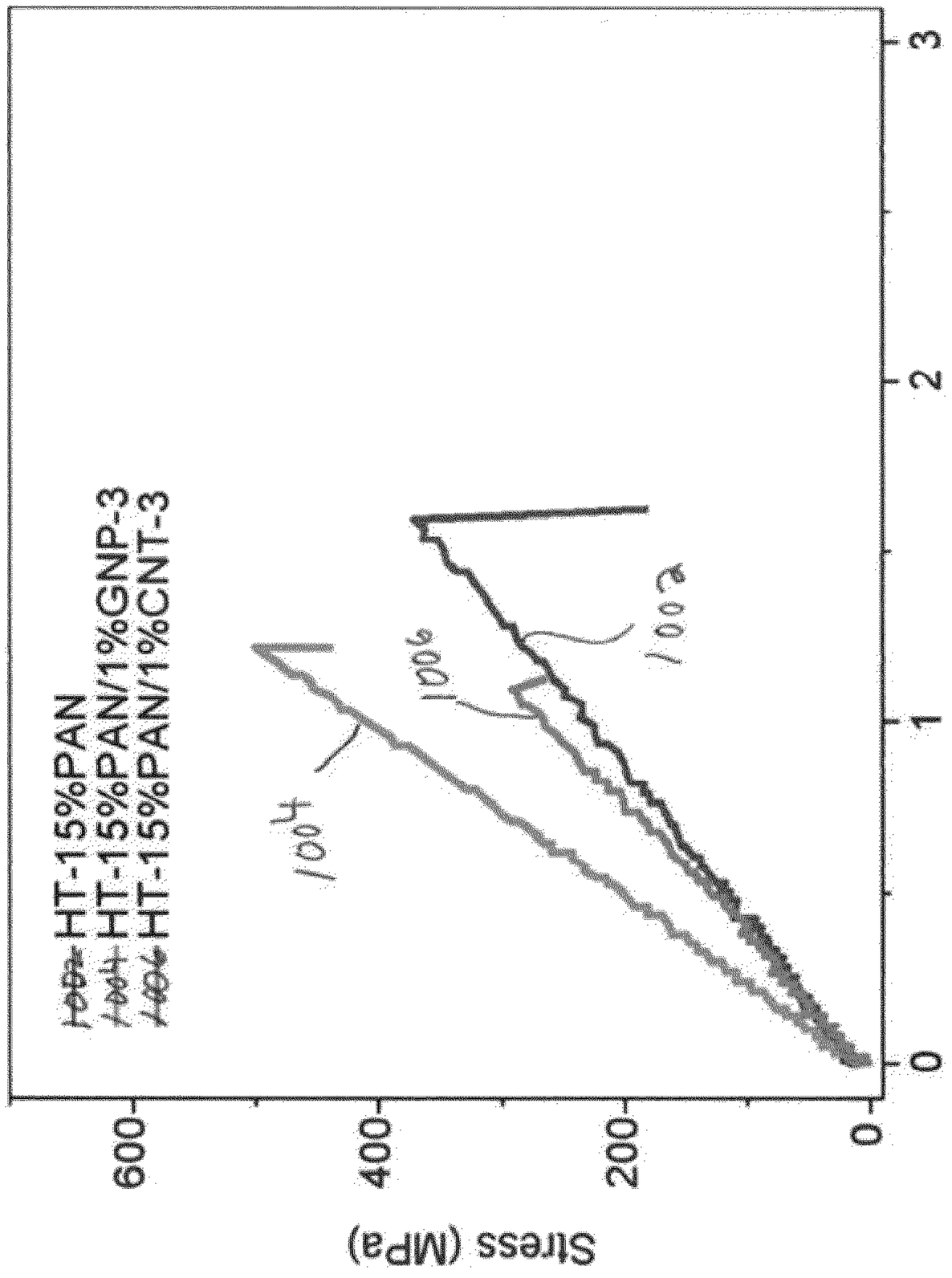
HT-15%PAN
HT-15%PAN/1%GNP-3
HT-15%PAN/1%CNT-3
100%
100%
100%
Stress (MPa)
600
400
200
0
0
1
2
3
Strain (%)

FIG. 10

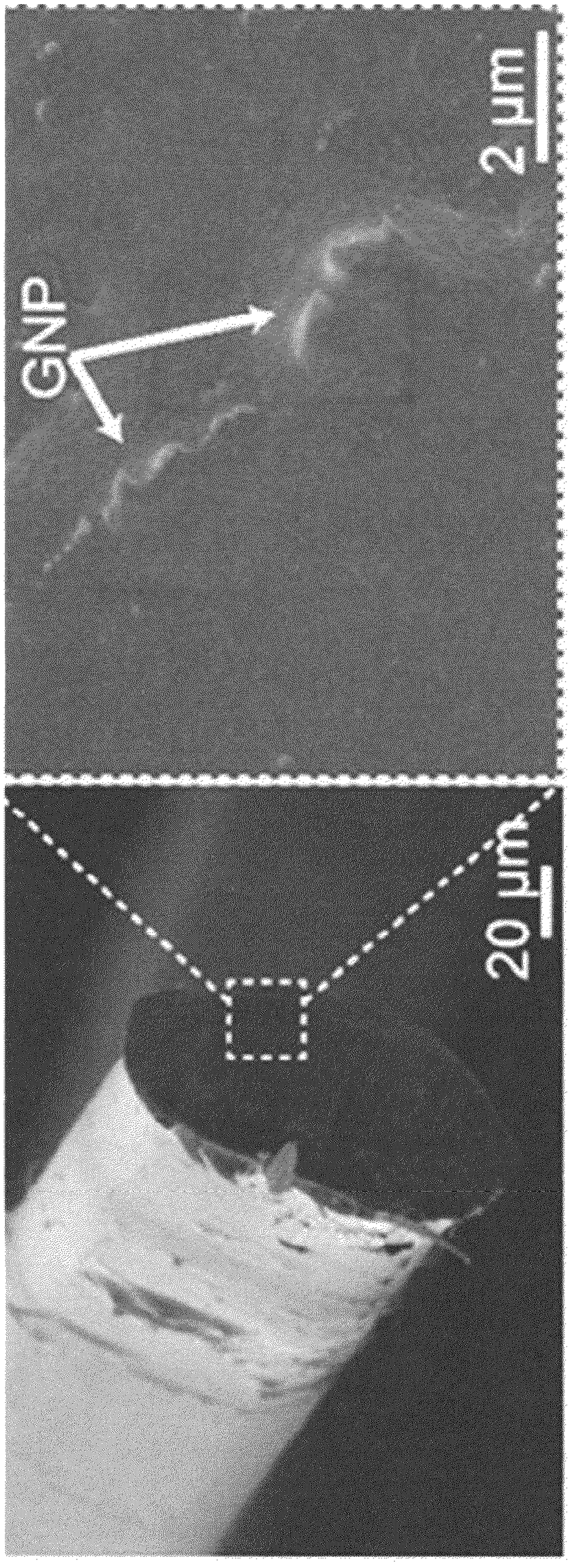

FIG. 11A

FIG. 11B

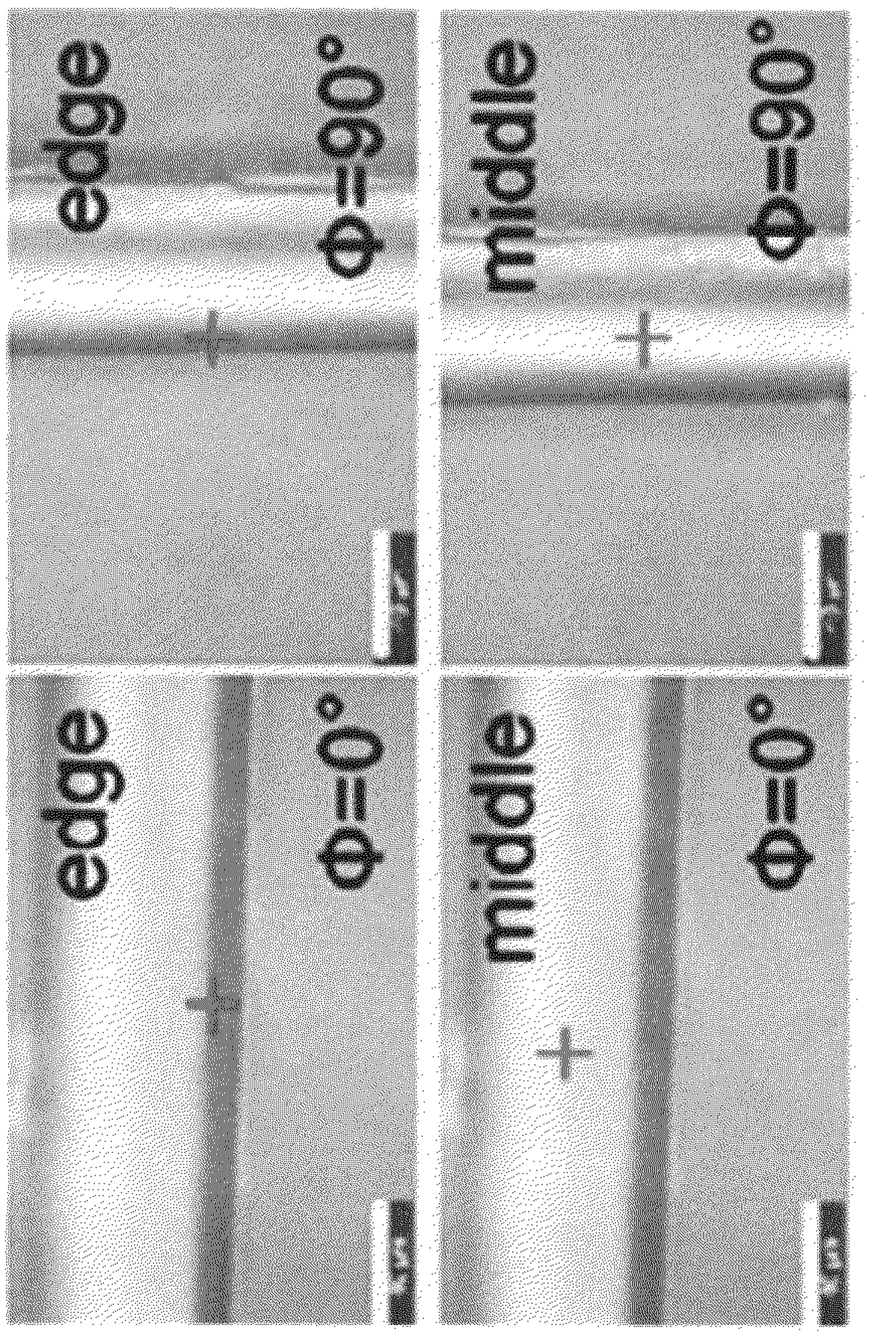

FIG. 11F FIG. 11G

FIG. 11D FIG. 11E

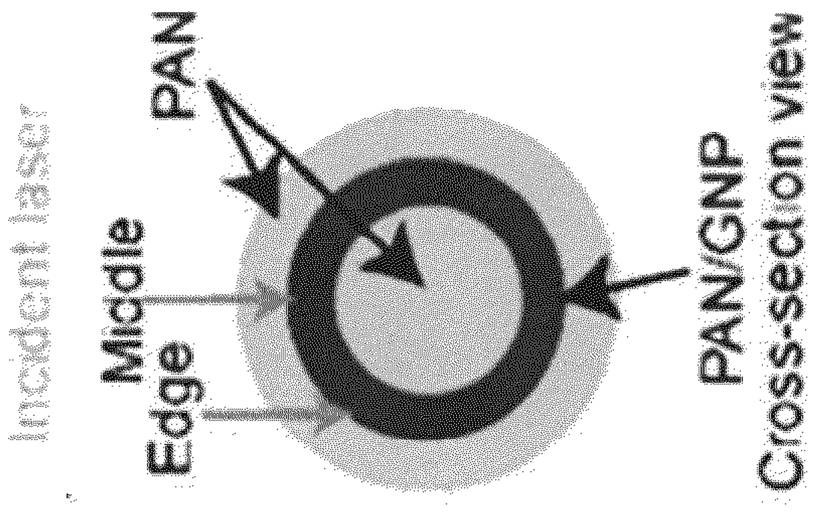

FIG. 11C

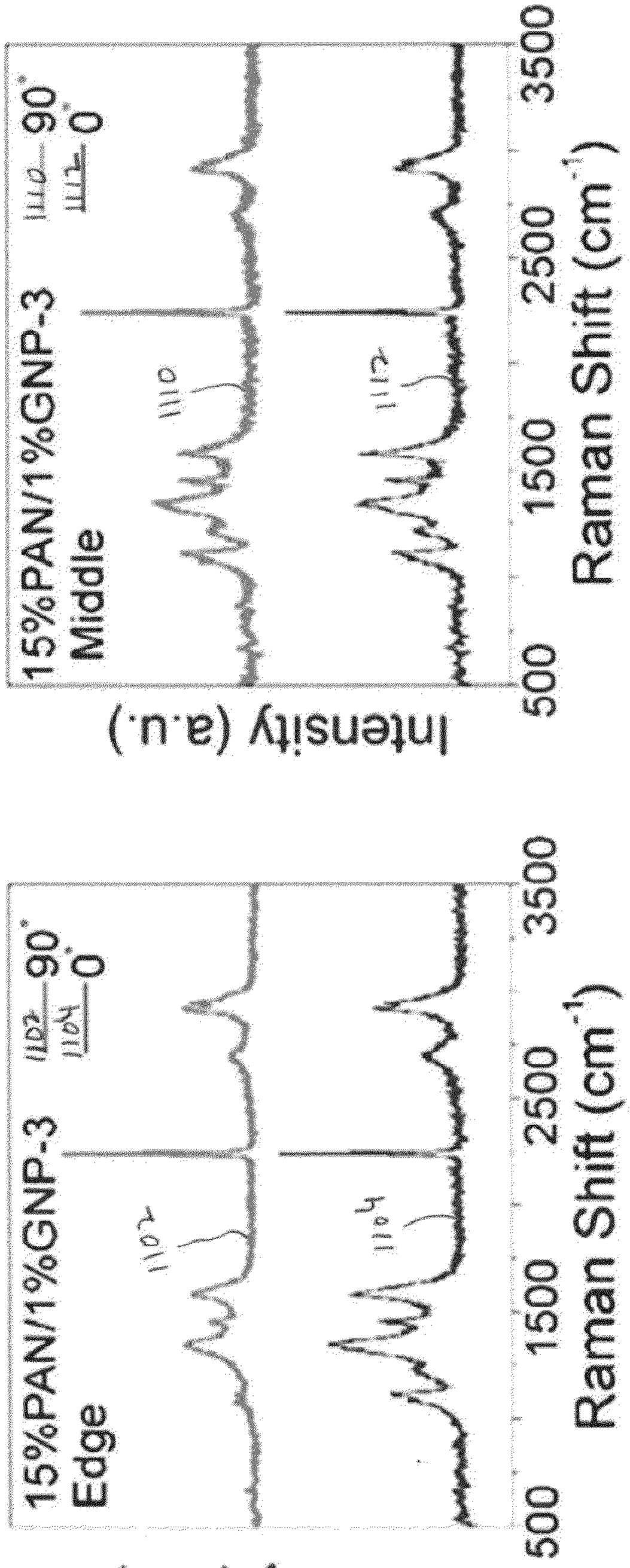

FIG. 11I

FIG. 11H

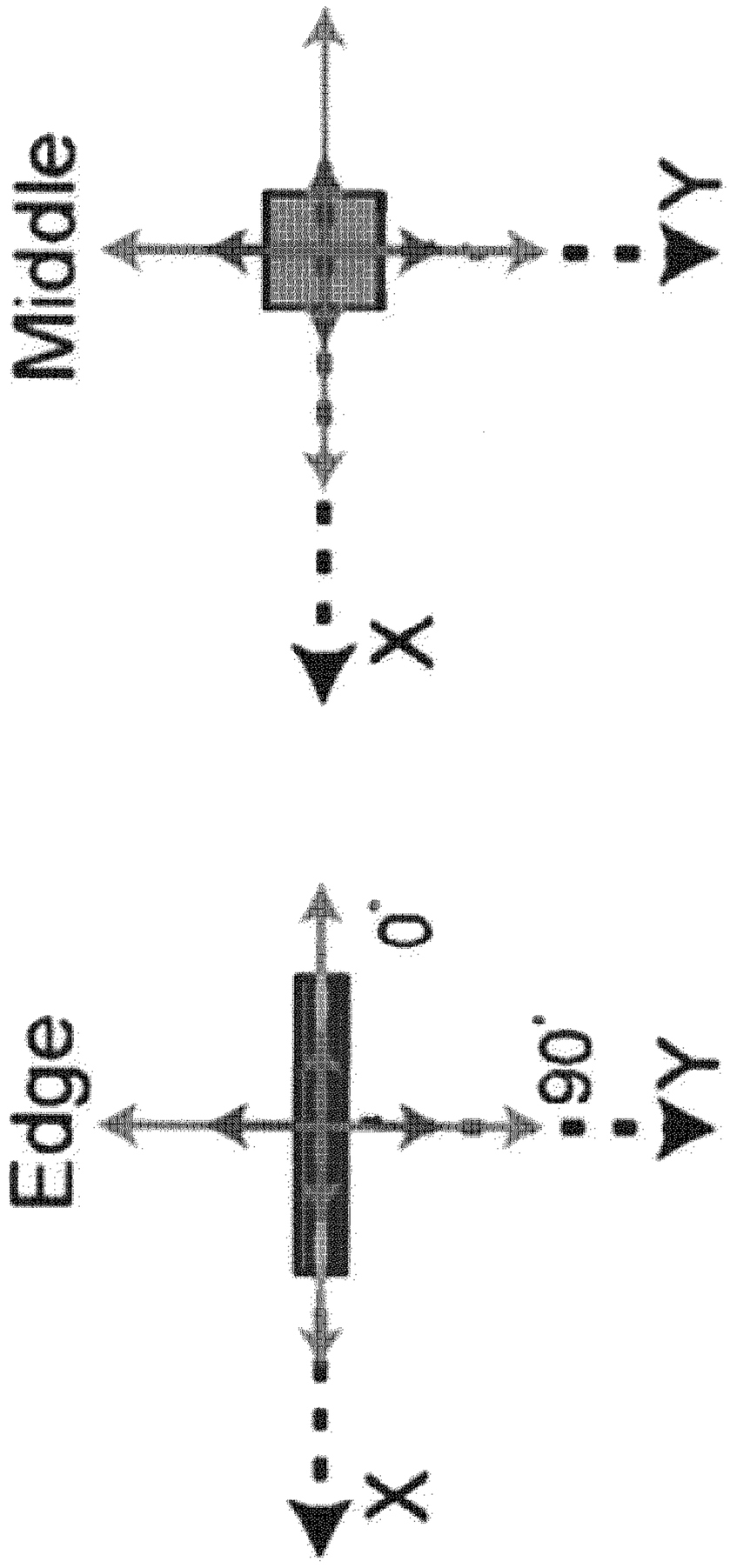

FIG. 11J

FIG. 11K

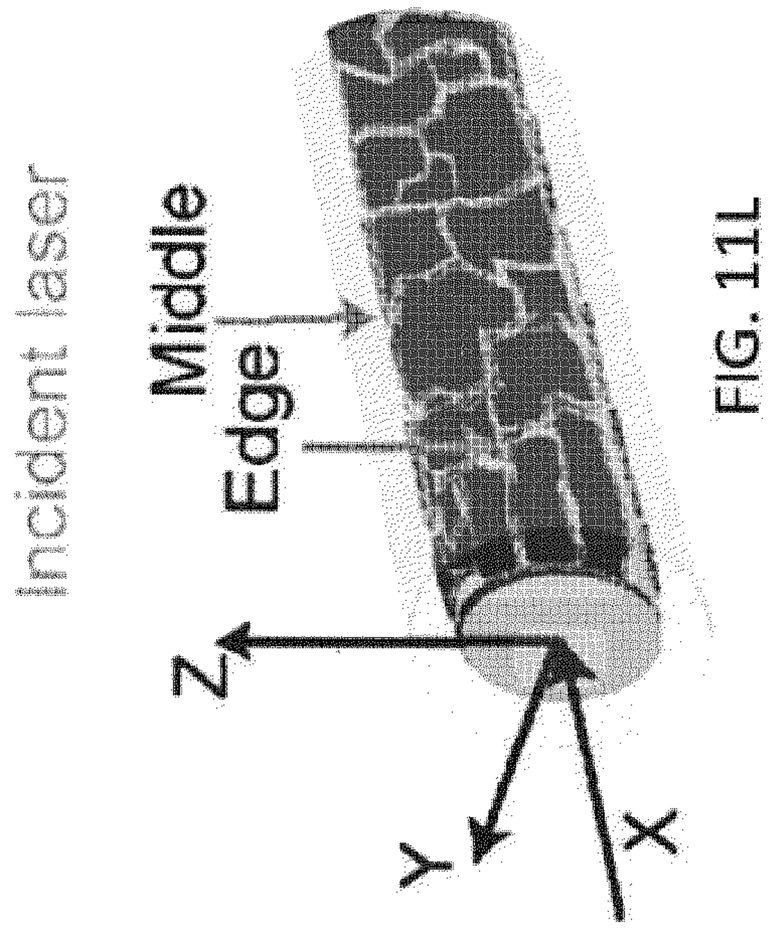

FIG. 11L

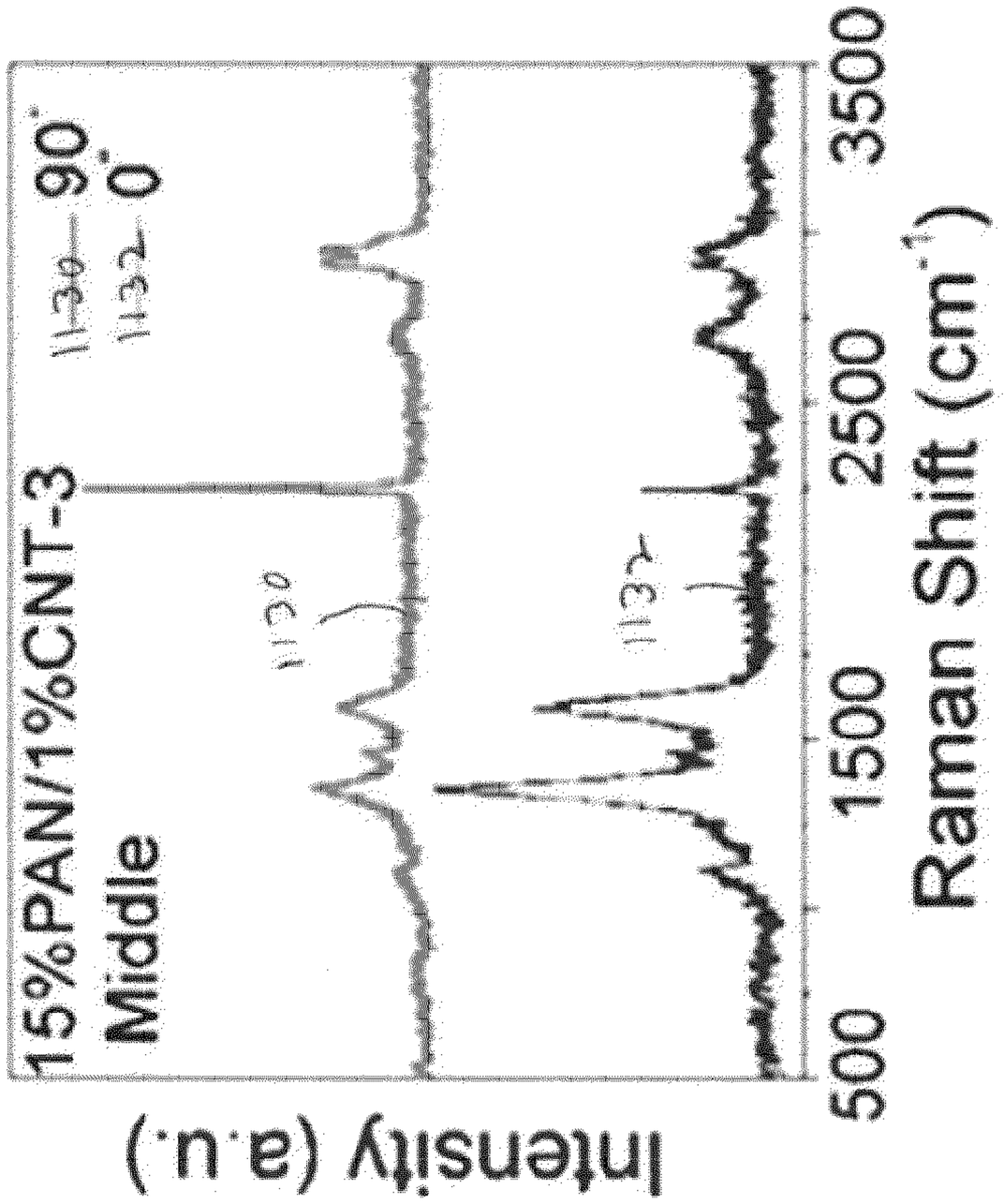

FIG. 11L

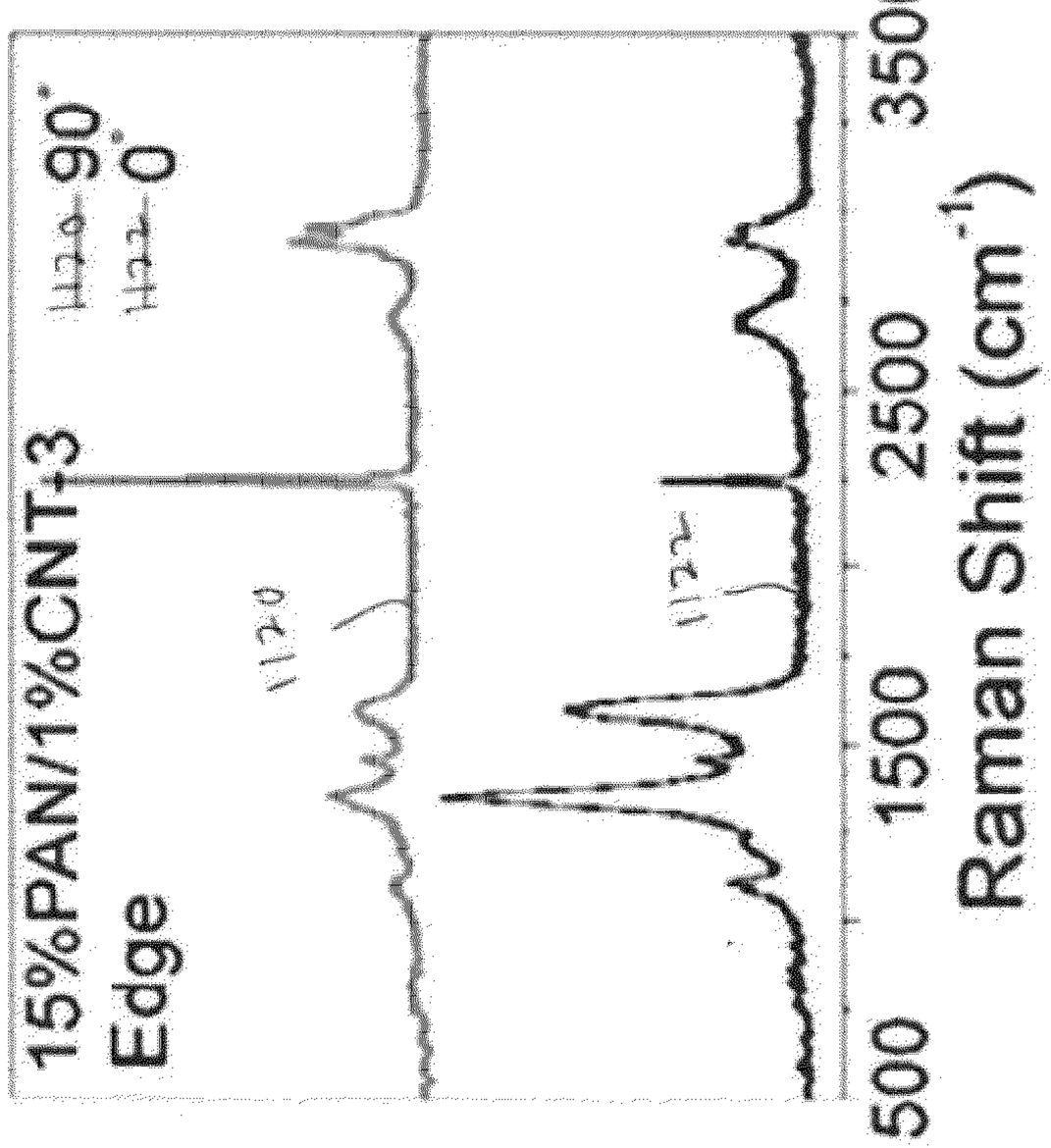

FIG. 11M

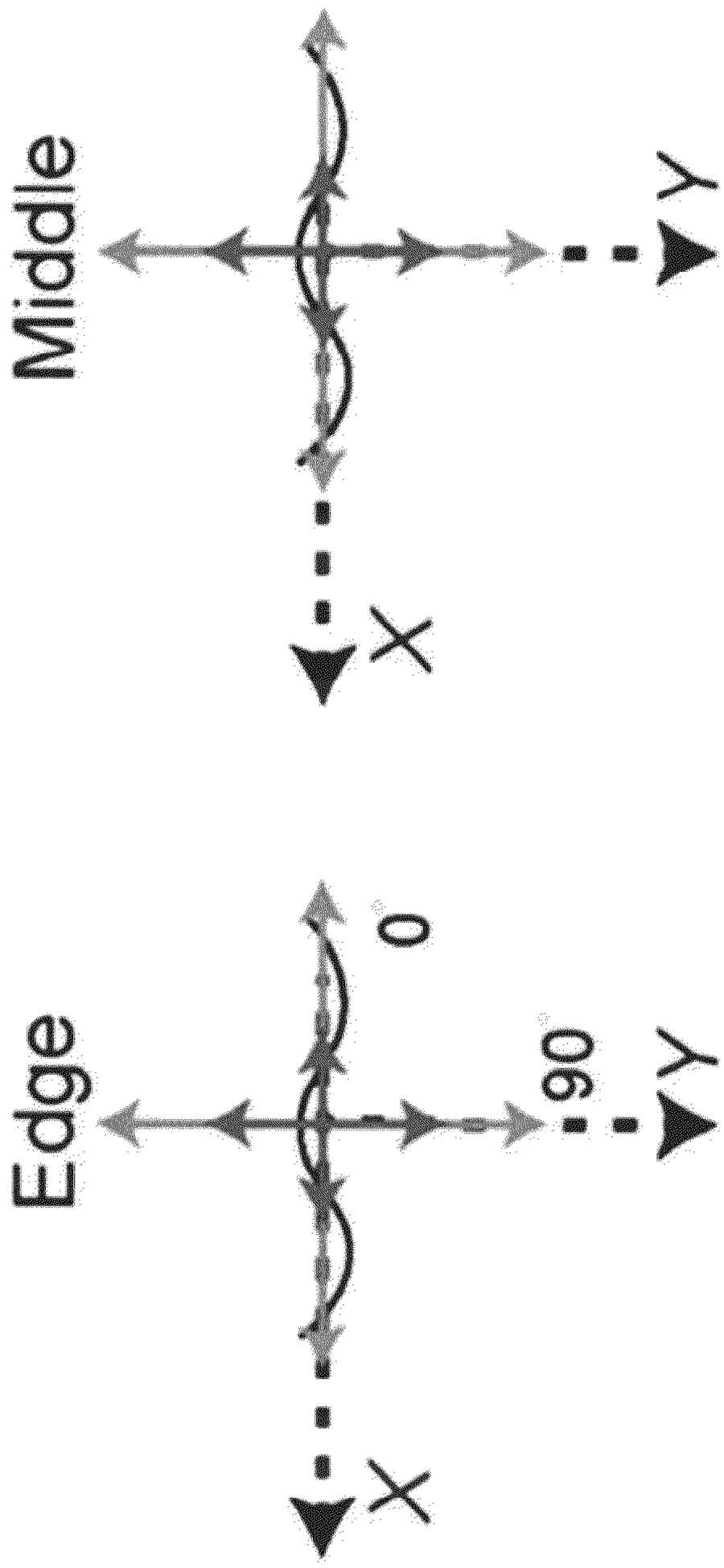

FIG. 12A

FIG. 12B

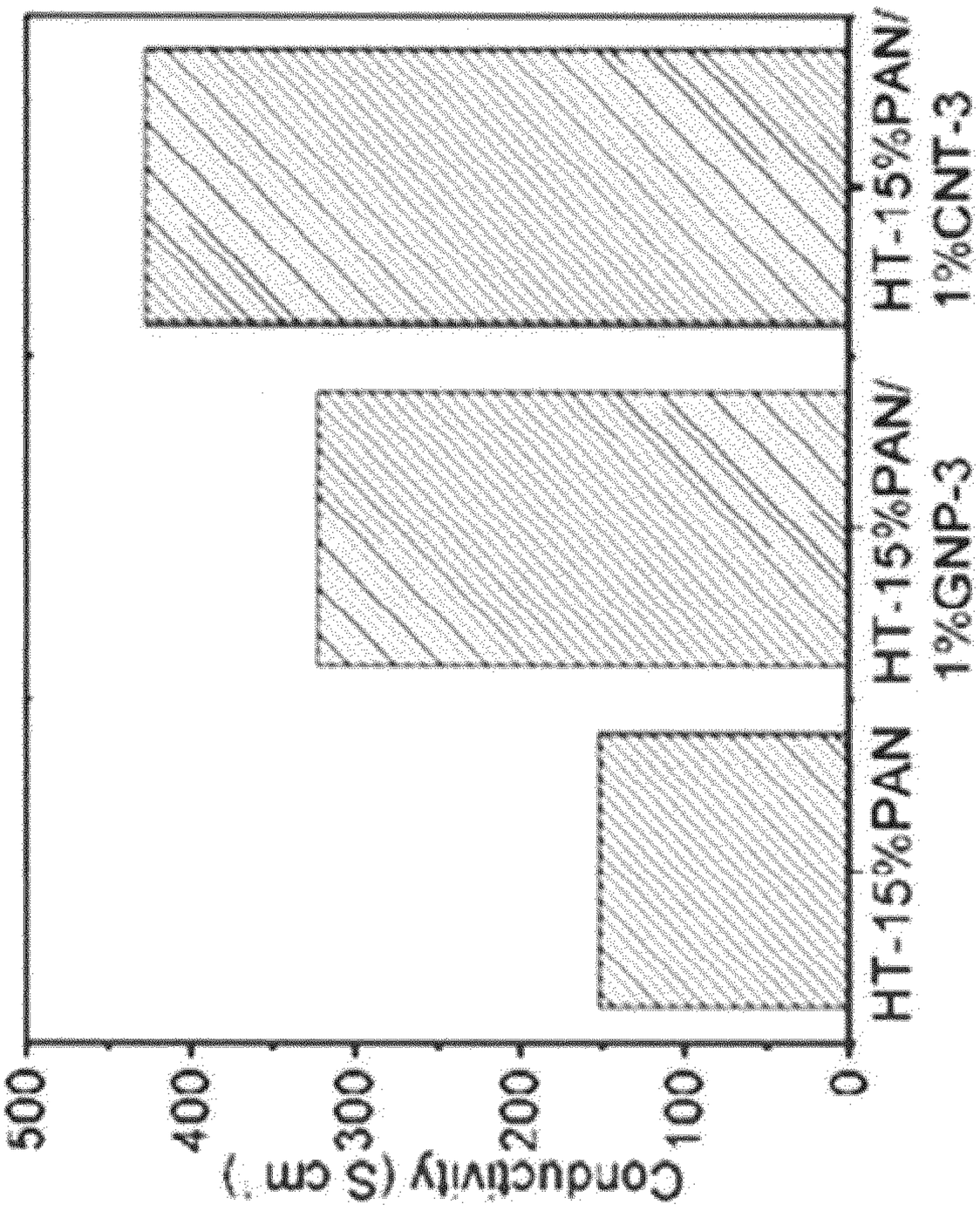
Conductivity (S cm⁻¹)
500
400
300
200
100
0
HT-15%PAN
HT-15%PAN/ 1%GNP-3
HT-15%PAN/ 1%CNT-3

FIG. 13A

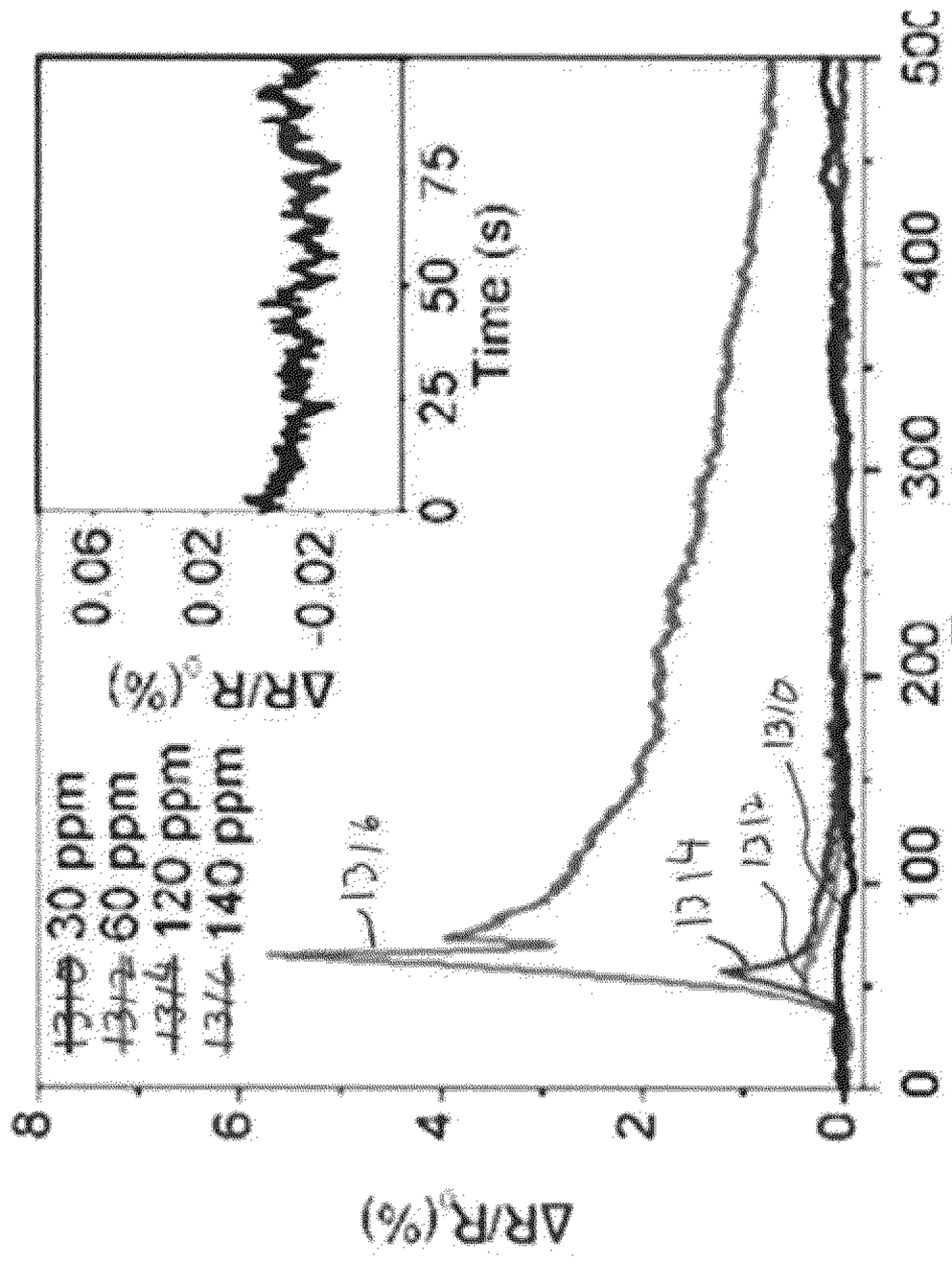

FIG. 13C

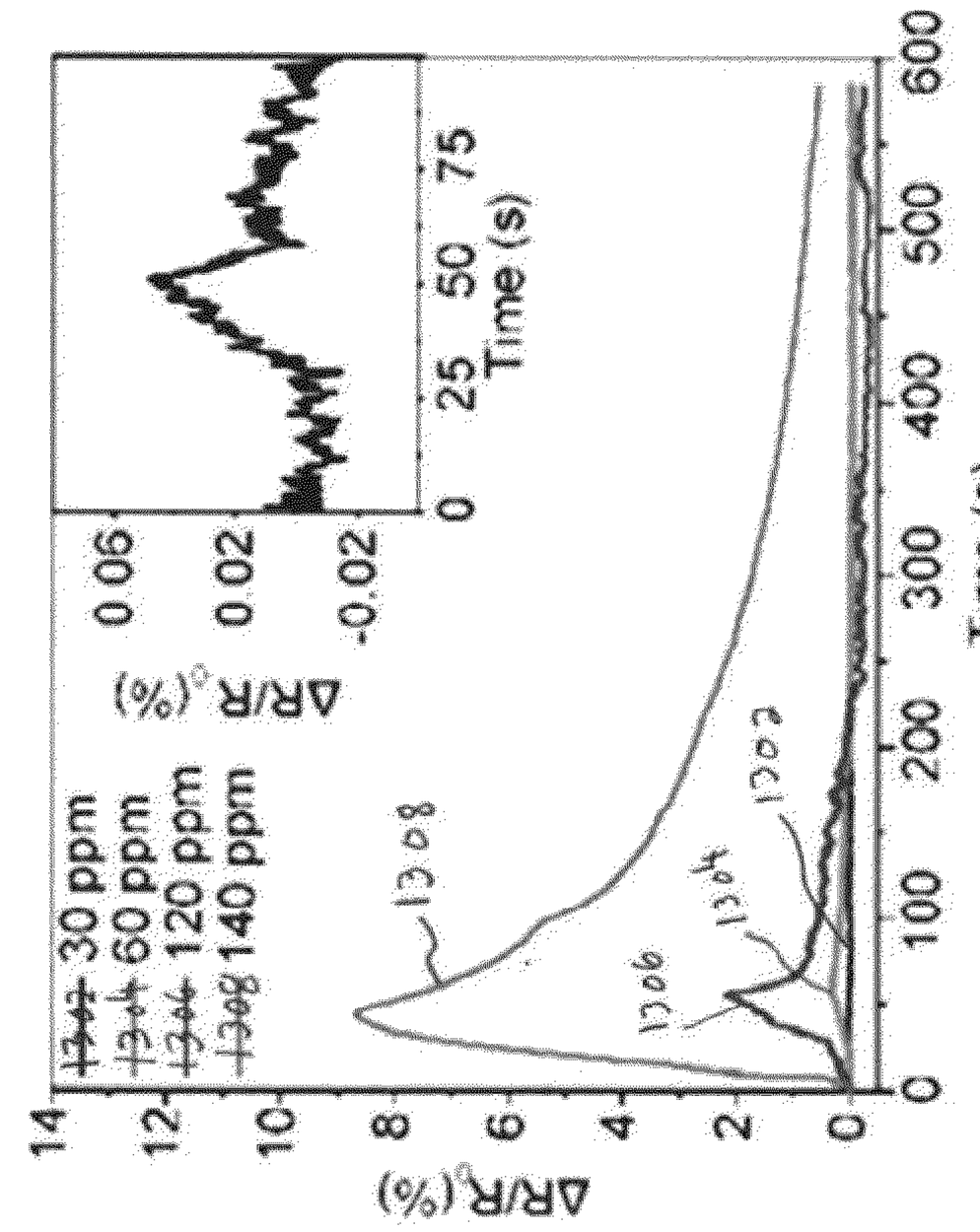

FIG. 13B

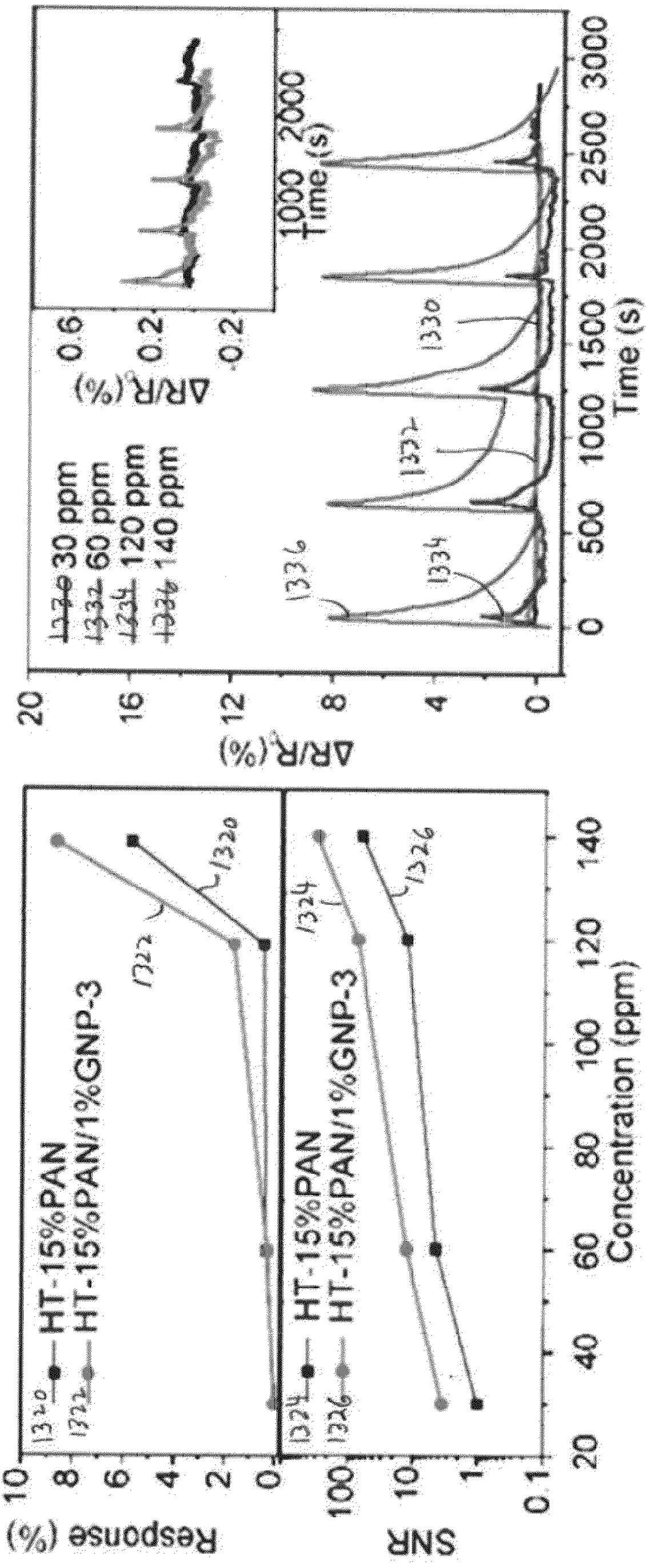

FIG. 13E

FIG. 13D

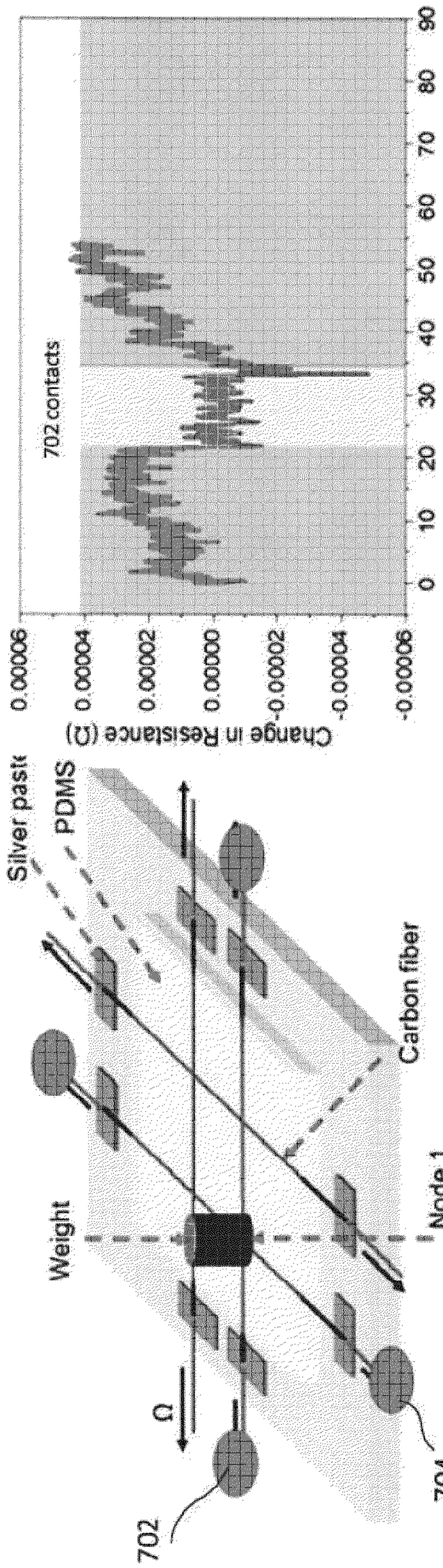

FIG. 14A

FIG. 14B

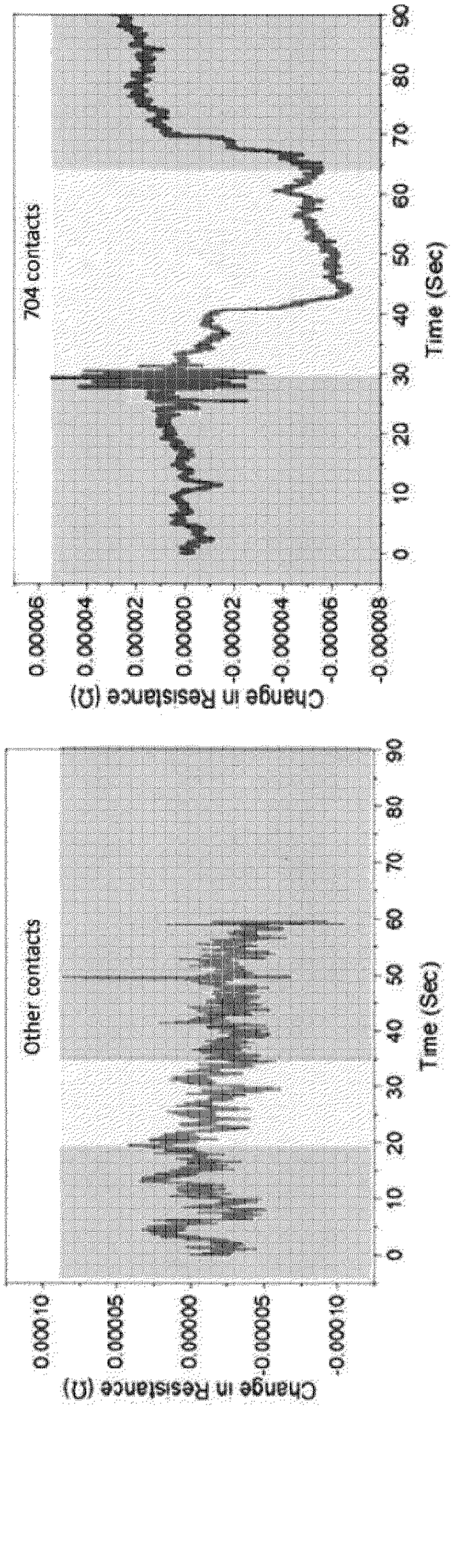

FIG. 14C

FIG. 14D

DRY-JET WET-SPINNING OF MULTIFUNCTIONAL CARBON FIBERS

CROSS-REFERENCE TO RELATED APPLICATION

[0001] This application claims the benefit of U.S. Pat. Application 63/285,306 filed on Dec. 2, 2021, which is incorporated herein by reference in its entirety.

STATEMENT OF GOVERNMENT SUPPORT

[0002] This invention was made with government support under 1902172 awarded by the National Science Foundation. The government has certain rights in the invention.

TECHNICAL FIELD

[0003] This invention generally relates to carbon fiber materials and dry-jet-wet-spinning of multifunctional carbon fibers.

BACKGROUND

[0004] Carbon fibers can be made from carbonized precursors, including cellulose, lignin, pitch, polyacrylonitrile (PAN), or Kevlar®. Processing parameters that can affect carbon fiber manufacturing include atmosphere effects, precursor type influences (viscose rayon fibers, PAN fibers, and isotropic pitch), and material sustainability (precursors from cellulose or lignin).

[0005] Properties exhibited by carbon fibers include physical strength, light weight, a low temperature of thermal expansion, chemical and biological inertness, high vibration damping, and high corrosion resistance. Carbon fibers have been used in the manufacture of a wide variety of products including sporting goods equipment, aerospace equipment, road and marine transport parts, medical devices, machine parts, and chemical processing equipment. Due to their mechanical and electrical properties, carbonized fibers have also been widely used in sensors, supercapacitors, actuators, electrodes, and filtration devices.

SUMMARY

[0006] Methods for producing multilayer and multifunctional carbonized coaxial composite fibers with precise interfacial engineering for graphene morphology control are described. These methods include carbonization of polyacrylonitrile (PAN)-precursor fibers (e.g., from PAN with a molecular weight of about 230,000 g/mol) and the inclusion of graphitic layers (e.g., from graphene nanoplatelets, graphene nanoribbons, graphene nanochips, or a combination thereof). A spinning method produces a three-layered fiber that utilizes the interfacial interactions between each layer for graphene alignment between graphitic layers. In particular, a 3D printed spinneret with optimized channel structures and dimensions is employed to embed graphitic layers in PAN-based fibers. By incorporating polymers and carbon nanoparticles in separate phases, coaxial layers can be formed along the fibers. Fibers with the inclusion of 1 wt% graphene nanoplatelets (GNPs) show improved mechanical properties relative to the pure PAN fibers after carbonization. Tension-free heat-treatment is utilized during stabilization and carbonization. The resulting carbonized fibers have hybrid structures between PAN- (e.g., turbostratic) and pitch-based (e.g., graphitic) fibers, and can be used in sensors that are efficiently responsive to, for example, chemical gases and mechanical pressures. This composite containing oriented GNPs improves modulus and increases electrical conductivity for enhancing volatile organic compounds (VOCs) sensing behaviors.

[0007] In a general aspect, a carbonized coaxial composite fiber includes an inner layer including carbonized polyacrylonitrile, a middle layer surrounding the inner layer and including carbonized graphene nanomaterials, and an exterior layer surrounding the middle layer including carbonized polyacrylonitrile. The graphene nanomaterials include graphene nanoplatelets, graphene nanoribbions, graphene nanochips, or any combination thereof. The carbonized graphene nanomaterials can be aligned along a length of the coaxial composite fiber.

[0008] Implementations of the general aspect can include one or more of the following features.

[0009] In some cases, the middle layer further includes carbonized polyacrylonitrile. The middle layer can be formed from a mixture including the polyacrylonitrile and the graphene nanomaterials, and a weight ratio of the polyacrylonitrile to the graphene nanomaterials in the mixture can be in a range of 1:15 to 15:1. In some implementations, the middle layer defines voids between the carbonized graphene nanomaterials. The voids can be at least partially filled with polyacrylonitrile. In some cases, the inner layer and the outer layer include polyacrylonitrile. In some implementations, a diameter of the coaxial composite fiber is in a range of about 50 microns to about 500 microns. A diameter of the inner layer can be in a range of about 20 microns to about 80 microns. In some cases, a thickness of the middle layer is in a range of about 20 microns to about 10 microns. In some implementations, a thickness of the outer layer is in a range of about 10 microns to about 50 microns.

[0010] Forming the coaxial composite fiber of the general aspect includes forming a coagulated gel precursor fiber by extruding a multiplicity of solutions through a multiphase spinneret through an air gap and into a solvent, hot drawing the coagulated gel precursor fiber to yield a drawn precursor fiber, oxidizing the drawn precursor fiber to yield a stabilized fiber, and carbonizing the stabilized fiber to yield the coaxial composite fiber. The coagulated gel precursor fiber can include an inner layer including polyacrylonitrile, a middle layer including graphene nanomaterials, and an outer layer including polyacrylonitrile. The graphene nanomaterials can include graphene nanoplatelets, graphene nanoribbons, graphene nanochips, or any combination thereof. In some cases, the multiplicity of solutions includes a first solution, a second solution, and a third solution corresponding to the inner layer, the middle layer, and the outer layer, respectively. The first solution and the third solution can include polyacrylonitrile. In some implementations, the first solution and the third solution are the same. The second solution can include graphene nanomaterials. In some cases, the second solution further includes polyacrylonitrile. In some implementations, a weight ratio of the polyacrylonitrile to the graphene nanomaterials is in a range of 1:15 to 15:1. In some cases, the first solution, the second solution, and the third solution include dimethylformamide. The solvent can include methanol. In some implementations, hot drawing the coagulated gel precursor fiber includes heating the coagulated gel precursor fiber above the glass transition temperature of polyacrylonitrile.

[0011] The details of one or more embodiments of the subject matter of this disclosure are set forth in the accompanying drawings and the description. Other features, aspects,

and advantages of the subject matter will become apparent from the description, the drawings, and the claims.

BRIEF DESCRIPTION OF DRAWINGS

[0012] The patent or application file contains at least one drawing executed in color. Copies of this patent or patent application publication with color drawing(s) will be provided by the Office upon request and payment of the necessary fee.

[0013] FIG. **1** shows the manufacturing of 3-layer carbonized coaxial composite fibers and post-treatment at three stages (drawing, stabilization, and carbonization).

[0014] FIGS. **2**A and **2**B are photographs of the 3D printed multiphase spinneret.

[0015] FIG. **3** shows the stabilization and carbonization procedure.

[0016] FIGS. **4**A - **4**L show cross-sectional scanning electron microscopy (SEM) images of the pre-carbonized and post-carbonized graphene nanoplatelets/polyacrylonitrile (GNP/PAN) fibers. The samples are: 0%PAN/10%GNP-3 pre-carbonized (FIG. **4**A), post-carbonized (FIG. **4**B), and expanded view post-carbonized (FIG. **4**C); 5%PAN/10% GNP-3 pre-carbonized (FIG. **4**D), post-carbonized (FIG. **4**E), and expanded view post-carbonized (FIG. **4**F); 10% PNA/10%GNP-3 pre-carbonized (FIG. **4**G), post-carbonized (FIG. **4**H), and expanded view post-carbonized (FIG. **4**I); 15%PAN/1%GNP-3 pre-carbonized (FIG. **4**J), post-carbonized (FIG. **4**K), and expanded view post-carbonized (FIG. **4**L).

[0017] FIGS. **5**A-**5**C show scanning electron microscopy (SEM) images of 15%PAN pre-carbonization (FIG. **5**A) and post-carbonization (FIGS. **5**B and **5**C). FIG. **5**C is an enlarged view of the region enclosed by the rectangle in FIG. **5**B. FIGS. **5**D-**5**F show SEM images of 15%PAN/1% carbon nanotubes (15%PAN/1%CNT-3) pre-carbonization (FIG. **5**D and post-carbonization (FIGS. **5**E and **5**F). FIG. **5**F is an enlarged view of the region enclosed by the rectangle in FIG. **5**E.

[0018] FIGS. **6**A and **6**B show SEM images of 15%PAN/1%GNP-D before carbonization. FIG. **6**B is an expanded view of the rectangle in FIG. **6**A. FIGS. **6**C and **6**D show SEM images of 15%PAN/1%GNP-D after carbonization. FIG. **6**D is an enlarged view of the region enclosed by the rectangle in FIG. **6**C.

[0019] FIGS. **7**A-**7**C show differential scanning calorimetry (DSC) curves of different heating rates in nitrogen for 15%PAN (FIG. **7**A), 0%PAN/10%GNP-3 (FIG. **7**B), and 10%PAN/10%GNP-3 (FIG. **7**C). FIGS. **7**D-**7**F show differential scanning calorimetry (DSC) curves of different heating rates in air for 15%PAN (FIG. **7**D), 0%PAN/10%GNP-3 (FIG. **7**E), and 10%PAN/10%GNP-3 (FIG. **7**F). FIGS. **7**G-**7**I show plots of $\ln(\varphi/T_m^2)$ versus $1/T_m$ according to Kissinger method for activation energies of (FIG. **7**G) cyclization, (FIG. **7**H) oxidation, and (FIG. **7**I) crosslinking reactions.

[0020] FIGS. **8**A and **8**B show mechanical properties of effect of increasing PAN concentration in the middle layer (FIG. **8**A) and comparison between 15%PAN and 1 wt% loading of nanoparticles with and without layered structures (FIG. **8**B).

[0021] FIG. **9** shows Raman spectra of the carbonized 10%PAN/10%GNP-3 fiber across a fiber cross-section. These spectra were deconvolutions through Gauss-Lorentz fitting after subtraction of the baseline.

[0022] FIG. **10** shows stress-strain curves after carbonization.

[0023] FIG. **11**A shows a cross-sectional SEM image of the 15%PAN/1%GNP-3. FIG. **11**B is an the enlarged view of the region enclosed by the rectangle in FIG. **11**A showing aligned GNP. FIG. **11**C shows a schematic of the two Raman incident points on the middle and edge of the middle layer of the carbon fibers. FIGS. **11**D-**11**G are the optical images showing the rotation of 0° and 90° for both sections. FIGS. **11**H and **11**I show the corresponding Raman signal for the edge and middle sections, respectively, for 15%PAN/1% GNP-3. FIGS. **11**J - **11**L are the schematics for the orientations of GNP. FIGS. **11**M and **11**N show the corresponding Raman signal for the edge and middle sections, respectively, for 15%PAN/1%CNT-3.

[0024] FIGS. **12**A and **12**B depict the orientation of 1D CNT for edge section and or middle section, respectively. Raman intensities showed angular dependency for both positions due to 1D nature of CNTs.

[0025] FIGS. **13**A - **13**E show the electrical and volatile organic compound (VOC) sensing performances of carbon fibers. FIG. **13**A shows the conductivity of three selected carbonized fibers at 1250° C. FIGS. **13**B and **13**C show the chemoresistive response of hot drawn, stabilized, and carbonized (designated "HT") HT-15%PAN/1%GNP-3 and HT-15%PAN fibers, respectively, to various concentrations of methanol for 30 seconds. The enlarged sections are the response for 30 ppm concentration. FIG. **13**D shows the response magnitude and their SNR with increasing concentrations for the two tested fibers. FIG. **13**E shows the cyclic performances of the HT-15%PAN/1%GNP-3 with various methanol concentrations.

[0026] FIG. **14**A shows a schematic of the pressure sensor test setup. FIGS. **14**B-**14**D show signals collected along path **702** (FIG. **14**B), **704** (FIG. **14**C), and **706** (FIG. **14**D).

DETAILED DESCRIPTION

[0027] Methods for producing multilayer and multifunctional carbonized coaxial composite fibers with precise interfacial engineering for graphene morphology control are described. These methods include carbonization of polyacrylonitrile (PAN)-precursor fibers (e.g., from PAN with a molecular weight of about 230,000 g/mol) and the inclusion of graphitic layers from graphene nanomaterials (e.g., graphene nanoplatelets, graphene nanoribbons, graphene nanochips, or a combination thereof). A spinning method produces a three-layered fiber that utilizes the interfacial interactions between each layer for graphene alignment between graphitic layers. In particular, a 3D printed spinneret with optimized channel structures and dimensions is employed to embed graphitic layers in PAN-based fibers. By incorporating polymers and carbon nanoparticles in separate phases, coaxial layers can be formed along the fibers. Fibers with the inclusion of 1 wt% graphene nanoplatelets (GNP) show improved mechanical properties relative to the pure PAN fibers after carbonization. Tension-free heat-treatment is utilized during stabilization and carbonization. The resulting carbonized coaxial composite fibers have hybrid structures between PAN- (e.g., turbostratic) and pitch-based (e.g., graphitic) fibers, and can be used in sensors that are efficiently responsive to, for example, chemical gases and mechanical pressures. This composite containing oriented GNPs improves modulus and increases electrical conductivity for enhancing volatile organic compounds (VOCs) sensing behaviors.

[0028] A spinning method produces a three-layered fiber that utilizes the interfacial interactions between each layer for graphene alignment between graphitic layers. In particular, a 3D printed spinneret with optimized channel structures and dimensions is employed to embed graphitic layers in PAN-based fibers. By incorporating polymers and carbon nanoparticles in separate phases, coaxial layers can be formed along the fibers.

[0029] FIG. **1** depicts the process **100** for manufacturing 3-layer carbonized coaxial composite fibers. The transformation of precursor PAN fibers to coaxial composite carbon fibers includes oxidative stabilization, carbonization, and graphitization. Syringe pumps **102**, **104**, and **106** drive the plungers of syringes **108**, **110**, and **112**, respectively, to force the spinning dope solutions **114**, **116**, and **118** into a three channel multiphase spinneret **120** configured to form the inner layer **122**, the middle layer **124**, and the outer layer **126**, respectively, of the carbonized coaxial composite fiber **128**. In one example, the inner layer spinning dope solution **114** and the outer layer spinning dope solution **118** include a PAN-N,N-dimethylformamide (PAN-DMF) solution. In some cases, the inner layer and the outer layer spinning dope can be the same solution. The composition of the middle layer spinning dope **116** can include PAN, DMF, graphene nanomaterials, and carbon nanotubes (CNTs). In one example, the middle layer is formed from a mixture including PAN and graphene nanoplatelets (GNPs), and a weight ratio of the PAN to the graphene nanoplatelets in the mixture is in a range of 1:15 to 15:1. Each of the 3 three spinning dope solutions enter separately into channels **130**, **132**, and **134** of the multiphase spinneret **120**. The 3 spinning dope solutions exit the multiphase spinneret **120** as a precursor fiber **136** with inner, middle, and outer layers. The precursor fiber **136** passes through an air gap **138** during which polymer chain extension, crystallization, and alignment can occur before forming gels with physically cross-linked macromolecules. The precursor fiber **136** is fed through a DMF/methanol coagulation bath **140** to form a coagulated gel precursor fiber **142**. The coagulated gel precursor fiber **142** is hot drawn at incrementally increased temperatures using a hot plate **146** to form a drawn precursor fiber **148** with maximized molecular extension. In some cases, hot drawing the coagulated gel precursor fiber **142** includes heating the coagulated gel precursor fiber **142** above the glass transition temperature of PAN.

[0030] Oxidative stabilization is performed on the drawn precursor fiber **148** to form a stabilized fiber **150**. The oxidative stabilization is performed in an oxidative atmosphere of dry air provided by dry air source **152** in a temperature range of 200° C. - 300° C., with or without applied tension F. This oxidative stabilization facilitates production of an oxidized ladder polymer parallel to the fiber axis by the cyclization of the pendant nitrile groups and the incorporation of oxygen.

[0031] Carbonization of the stabilized fiber **150** to form the carbonized coaxial composite fiber **128** is typically implemented in an atmosphere of nitrogen gas provided by nitrogen source **154** in the range of 400° C. -1500° C., with or without applied tension F. During this pyrolysis, non-carbon elements are removed as volatile products, the amounts varying with the temperature and gases evolved, which can include HCN, NH_3, N_2, H_2O, CO_2, CH_4, and H_2. The resulting carbon fibers typically have around 50% of the original fiber mass. End-to-end joining of cyclized regions, aromatization of non-cyclized regions, and side-by-side condensation reactions between laddered structures, which can result in broader heterocyclic regions, are observed. Dehydrogenation and denitrogenation can take place at a temperature of about 1000° C., giving rise to carbon ribbons containing limited N mass. The resulting carbon layer-plane packing can be enhanced with increased temperature treatments.

[0032] Graphitization is typically executed in an inert atmosphere above 2000° C. with applied tension for the non-graphitizing materials to be graphitized. PAN-based fibers are in the form of turbostratic graphite even after graphitization, at least because the helical crystal structure lacks a definite crystallographic arrangement of layer planes in terms of 3D stacking. Graphitization treatment, even at a high temperature of 2500° C. in argon, typically does not generate stacked graphene layers, as seen in pitch-based carbon fibers. This can also contribute to the high strength of PAN-based fibers, due at least in part to graphitic plane entanglement, while pitch-based fibers have high modulus due to close packing density and high graphitic plane orientations.

[0033] Following carbonization, the carbonized coaxial composite fiber **128** includes an inner layer **122**, a middle layer **124** surrounding the inner layer **122**, and an outer layer **126** surrounding the middle layer **124**. The inner layer **122** includes carbonized polyacrylonitrile. The middle layer **124** includes carbonized graphene nanomaterials and can further include carbonized polyacrylonitrile. The carbonized graphene nanomaterials are aligned along a length of the coaxial composite fiber **128**. The middle layer **124** can define voids between the graphene nanomaterials. The voids can be at least partially filled with PAN. The outer layer **126** includes carbonized polyacrylonitrile. The diameter of the carbonized coaxial composite fiber **128** is in a range of about 50 microns to about 80 microns. The diameter of the inner layer **122** is in a range of about 20 microns to about 80 microns. The radial thickness of the middle layer **124** is in a range of about 20 microns to about 10 microns. The radial thickness of the outer layer **126** is in a range of about 10 microns to about 50 microns.

[0034] FIGS. **2**A and **2**B are photographs showing two views of the 3D printed spinneret **120**. The 3 spinning dope solutions enter channels **130**, **132**, and **134** and exit spinneret **120** through the outer opening **202**, middle opening **204**, and inner opening **206** to form the precursor fiber.

[0035] FIG. **3** is a plot of temperature applied to the fibers as a function of time during the stabilization and carbonization procedures. Fibers were heated starting from room temperature to 280° C. at a rate of 5° C./minute in air. The fibers were then held at a constant temperature of 280° C. for 90 minutes. Subsequently, air atmosphere was changed to nitrogen atmosphere and the fibers were heated at a rate of 5° C./min to 1250° C. The fibers then were held for at 1250° C. for 10 minutes before cooling.

EXAMPLES

[0036] Materials. The polyacrylonitrile (PAN) copolymer (i.e., 99.5% acrylonitrile/ 0.5% methacrylate in poly(acrylonitrile-co-methacrylic acid, with molecular weight 230,000 g/mol, and mean particle size of 50 μm, and) was obtained from Goodfellow Cambridge Limited, Huntingdon, England. Graphene nanoplatelets (GNPs) (i.e., surface area 120-150 m^2/g) were obtained from Sigma-Aldrich, and carbon nanotubes (CNTs) (i.e., NC 7000, with avg. diameter 9.5 nm, avg. length 1.5 μm, avg. surface area 250-300 m^2/g, carbon purity 90%, transition metal oxide < 1%, and volume resistivity measured on powder at 10^{-6} Ω/m) were obtained

from Belgium Nanocyl SA. In thermoplastics, the percolation threshold of electrical conductivity was reported to be 0.5 wt% to 4.5 wt%. N, N-dimethylformamide (DMF) as the dispersion solvent and methanol as the coagulant were obtained from Sigma-Aldrich. All materials were purchased and used as received without further modifications.

[0037] Manufacturing processes of fiber spinning and heat-treatment. Table 1 lists the terminology for manufactured fibers and their manufacturing details. The following sections describe the preparation of the spinning procedures for three types of fibers.

TABLE 1

Summary of fiber terminology, compositions, processability, and testability

		Compositions (wt%)				Processability and testability		
		Interior and Exterior Layers	Middle Layer					
Fiber type	Fiber Name	PAN to DMF		GNP	CNT	Spinnability#	Heat-treatment*	Mechanical testability+
1-phase	15%PAN	15	N/A	N/A	N/A	Y	Hot drawing at 110, 130, and 150° C.; stabilization at 280° C. for 1.5 hrs, carbonization at 1250° C. for 10 mins	Y
D-phase	15%PAN/1%GNP-D	15	N/A	1	N/A	Y		N
3-layer	0%PAN/10%GNP-3	15	0	10	0	Y		N
	5%PAN/10%GNP-3		5	10	0	Y		N
	10%PAN/10%GNP-3		10	10	0	Y		N
	15%PAN/10%GNP-3		15	10	0	N		N
	15%PAN/1%GNP-3		15	1	0	Y		Y
	15%PAN/1%CNT-3		15	0	1	Y		Y

Spinnability showing a viscosity of composition 15 wt%PAN/10 wt%GNP too high to spin fibers; Y, spinnable; N, not spinnable.

*All carbonized fibers have the designation 'HT' placed before the established terminology (e.g., HT-15%PAN) meaning the 15%PAN fibers were treated after hot drawing, stabilization, and carbonization.

+Feasibility of handing carbonized fibers during mechanical tests. Y= Yes; N= No

[0038] 1-phase PAN fibers: A 15 wt% PAN/DMF solution was made by dissolving 22.5 g PAN in 150 ml DMF at 85° C. under a mechanical stir for 2 hours until obtaining a transparent solution. The solution was then deaerated in a vacuum oven (Thermo Scientific Lindberg Blue M lab oven) for 1 hour. The bubble-free solution was carefully transferred to a metal syringe connected to a syringe pump followed by fiber spinning. The injection rate was at 2 ml/min.

[0039] D-phase PAN-nanoparticle composite fibers: A dispersion of GNP/DMF was first obtained through 20 minutes of tip sonication at 60% amplitude (Q500, Fisherbrand). The dispersion was added to the prepared PAN/DMF solution to obtain different GNP concentrations (e.g., 1 and 10 wt%) followed by 2 hours of stirring at 85° C. The mixture was then transferred to a metal syringe for further fiber spinning. The injection rate was at 2 ml/min.

[0040] 3-layer PAN/PAN-nanoparticle/PAN composite fibers: 3-layer fibers consisted of coaxial stacking layers. Referring to FIGS. **1**, **2**A, and **2**B, the multiphase spinneret **120** has three channels **130**, **132**, and **134** responsible for generating the inner layer, the middle layer, and outer layer, respectively, each of which was fed by one type of spinning dope. Both the inner layer and the outer layer were filled with 15 wt% PAN/DMF solutions with the same preparation procedures for the above-mentioned 1-phase PAN fibers. The composition of the middle layer varied based on the weight of polymers and nanoparticles added. The concentrations of PAN/DMF were 0, 5, 10, and 15 wt%. Both GNP/DMF and CNT/DMF suspensions were added to the pre-dissolved PAN/DMF solutions in a manner similar to that for the D-phase spinning dope, and they were labeled, as shown in Table 1. The injection rate of the syringe pump **104** was 1 ml/min for the middle channel and 2 ml/min for syringe pumps **102** and **106** for the interior channel and exterior channel, respectively.

[0041] Fiber spinning. Dry-jet wet-spinning as depicted in FIG. **1** was used to fabricate both the pure PAN and the PAN/nanoparticle composite fibers. The disclosed multiphase spinneret **120** was advantageous in positioning/placing polymers and nanoparticles at different layers. An air gap **138** of 2 cm was chosen for sufficient polymer chain extension, crystallization, and alignment before forming gels with physically crosslinked macromolecules. Solvent exchange was performed on the precursor fibers in a DMF/methanol coagulation bath **140** to increase fiber stiffness and facilitate their collection on fiber winders. The take-up speeds of different fibers, which varied due to their rheological behaviors, were chosen to be the highest rate possible without losing fiber continuity. These fibers were drawn at incrementally increased temperatures of 110° C., 130° C., and 150° C., consecutively, for a maximized molecular extension, and the corresponding draw ratios are listed in Table 2. Fibers were stabilized at 280° C. via the high-temperature tube furnace (Lindberg with a heating capacity of ~2000° C.) and carbonized at 1250° C., as shown in FIG. **3**. Fibers were heated by wrapping around an alumina boat. The properties of final fibers of 15%PAN, 15%PAN/1% GNP-3, and 15%PAN/1%CNT-3 tested. Other fibers were too brittle to be tested or further processed. The study of the morphologies of the 3-layer fibers with different polymer concentrations in the middle layers is advantageous in understanding the polymer-nanoparticle interactions as a function of their configurations and interfacial engineering for high-performance composites.

TABLE 2

Recorded draw ratios and resulting fiber diameter

		Draw Ratio (Dr)				
Types of fiber	Fiber name	110° C.	130° C.	150° C.	Dr_{Heat}	D (μm)
1-phase	15%PAN	1.6	2.5	2	8.0	108.0±3.4
D-phase	15%PAN/1%GNP-D	2.4	4.0	-	9.6	110.0±4.1
3-layer	0%PAN/10%GNP-3	1.4	1.9	2.5	6.7	191.40

TABLE 2-continued

Recorded draw ratios and resulting fiber diameter						
		Draw Ratio (Dr)				
Types of fiber	Fiber name	110° C.	130° C.	150° C.	Dr_{Heat}	D (μm)
						±5.3
	5%PAN/10%GNP-3	3.4	3.4	-	11.6	114.00±2.8
	10%PAN/10%GNP-3	2.0	2.0	2.0	8.0	65.70±3.5
	15%PAN/1%GNP-3	2.3	2.3	2.3	12.2	77.80±2.9
	15%PAN/1%CNT-3	5.3	2.3	2.3	28.0	77.80±3.1

[0042] Analysis. Differential Scanning Calorimetry (DSC) (DSC **250**, TA Instruments Inc., USA) was conducted on 3 mg fiber samples with different heating rates to 350° C. in a nitrogen atmosphere to understand the cyclization behaviors, followed by reruns in the air for oxidation and crosslinking studies. Single filament tensile tests were conducted using a tensile tester (Discovery HR-2 hybrid rheometer, TA Instruments Inc., USA). A constant linear strain rate of 150 μm/sec and a gauge length of 5 cm was used for the pre-carbonized fibers and a constant linear strain rate of 50 μm/sec and a gauge length of 1 cm was used for carbonized fibers. For each fiber composition, the mechanical properties of 5-10 samples were tested. Scanning Electron Microscopy (SEM) was used to characterize fiber morphology, performed on a Philips XL-30 Environmental SEM (operating voltage 10 kV). All fibers were fractured in liquid nitrogen and mounted on a 90° pin stub with the fractured end facing up for SEM imaging. All SEM samples were coated with a thin gold/palladium layer (15-20 nm) for image analysis of surface morphology, voids, and interfacial interactions. Electrical resistivity measurements of the pre- and post-heat-treated fibers were tested using a multimeter (Keithley DMM 7510). The resistivity as a function of chemical gases or mechanical pressures was monitored for sensing applications.

[0043] Fiber draw ratios. After collection via fiber winding, all the PAN and composite fibers were hot-drawn to maximize the polymer chain extension. The purpose of this hot-stage drawing was to achieve better graphitic plane packing and orientations during the post-spinning (i.e., stabilization, carbonization, and graphitization) of carbon fibers. The draw ratio of pure PAN fibers was 8.0, and a 1 wt% GNP inclusion increased this value to 9.6 in the composites. The presence of 10 wt% GNP in the middle layer significantly decreased the drawability to 6.7, mainly because of the defects (e.g., voids and loose packing of GNPs). An addition of PAN in this middle layer filled these defects and increased the interaction between the middle and neighbor layers, leading to increased draw ratios of 11.6 and 8.0 for a PAN concentration of 5 wt% and 10 wt%, respectively. After heating to 150° C., the drawn fibers also showed a consistent decrease in fiber diameters, namely, 191.4 μm for 0%PAN, 114.0 μm for 5%PAN, and 65.7 μm for 10%PAN in 10%GNP, suggesting the synergistic effects of including PAN/GNP of appropriate compositions (Table 3). However, a mixture of 15 wt%PAN/DMF and 10 wt% GNP/DMF in the middle layer was not spinnable at the 2 cm air-gap due to its low viscoelastic behavior (Table 1). A combination of 15%PAN/1%GNP and 15%PAN/1%CNT was used to examine the reinforcement effects.

TABLE3

Recorded draw ratios and resulting fiber diameter						
		Draw Ratio (Dr)				
Types of fiber	Fiber name	110°-C.	130°-C.	150°-C.	Dr_{Heat}	D (μm)
1-phase	15%PAN	1.6	2.5	2	8.0	108.0±3.4
D-phase	15%PAN/1%GNP-D	2.4	4.0	-	9.6	110.0±4.1
3-layer	0%PAN/10%GNP-3	1.4	1.9	2.5	6.7	191.40±5.3
	5%PAN/10%GNP-3	3.4	3.4	-	11.6	114.00±2.8
	10%PAN/10%GNP-3	2.0	2.0	2.0	8.0	65.70±3.5
	15%PAN/1%GNP-3	2.3	2.3	2.3	12.2	77.80±2.9
	15%PAN/1%CNT-3	5.3	2.3	2.3	28.0	77.80±3.1

[0044] SEM characterization. FIGS. **4**A-**4**L show cross-sectional SEM images of the 3-layers fibers with increasing PAN concentration before and after carbonization. For 0% PAN/10%GNP-3 and 5%PAN/10%GNP-3 fibers, prominent void spaces were observed in the middle layer before **402** and after **404** carbonization shown in FIGS. **4**A-**4**F. With the increase of PAN concentration, a more compact GNP morphology was observed for the middle layer of 10%PAN as shown in FIGS. **4**G-**4**I. The concentration of PAN in the middle layer had a significant effect on the GNP morphologies, resulting in more compact stacking and preferentially aligned GNP with an increase of PAN weight percentage, as observed in each of the enlarged regions. The layered and porous structure in the 0%PAN/10%GNP-3 fibers was formed according to the permeation rate determined by the following dynamic process. When thicker and denser PAN form gels above and below the GNP channel during spinning, the permeation rates would slow down due to the decreased accessibility to PAN materials in the middle layer (e.g., 5 wt%PAN < 10 wt%PAN < 15 wt% PAN in FIGS. **4**A, **4**D, and **4**G As a result, the less involvement of PAN in the middle layer led to more porous structures. A high concentration of PAN (e.g., 15 wt%) and low concentration of GNPs (e.g., 1 wt%) shown in FIGS. **4**J-**4**L, instead, had similar gelation kinetics between the most interior and exterior layers, resulting in densified microstructures without micropores as shown in FIG. **4**L. A similar structure could be observed for high PAN concentrations in the 15% PAN shown in FIGS. **5**A - **5**C and 15%PAN/1%CNT-3 fibers shown in FIGS. **5**D - **5**F. On the other hand, SEM images for the D-phase fiber (15%PAN/1%GNP-D) shown in FIGS. **6**A-**6**D indicated the formation of large GNP aggregates **602** throughout the fiber, resulting in a lower ratio, 9.6, compared to 12.2 of the 15%PAN/1%GNP-3 fiber. All 10% GNP-containing fibers exhibited graphitic middle layer structure after carbonization, resembling other reported graphene-based fibers (FIGS. **4**B, **4**E, and **4**H). However, voids also appeared which was likely due to the different mass loss between PAN polymer chains and the graphitic GNP nanoparticles. For 1% GNP-containing fibers, D-phase fiber showed much larger voids at the surface of the fractured cross-section shown in FIG. **6**C compared to the 3-phase fiber, which could be the main cause for its low survivability during carbonization, resulting in unsuccessful mechanical characterization.

[0045] Kinetic analysis. Thermal stabilization plays a role in PAN-based carbon fiber fabrication, which transforms

PAN polymer chains into stabilized ladder structure through oxidation, cyclization, and crosslinking reactions. As least in part because oxygen is used for the oxidation and crosslinking process, a separate monitoring strategy was used as the fibers were first run under nitrogen atmosphere to observe the cyclization process, followed by a rerun in the air to study the oxidation and crosslinking behaviors in the DSC. During these processes, different heating rates were used to monitor the kinetics and the associated activation energies. The single peak in the nitrogen atmosphere corresponds to the cyclization process (FIGS. **7**A-**7**C), and the two peaks in their corresponding reruns in the air represent the oxidation and crosslinking processes (FIGS. **7**D-**7**F). The peak temperatures of cyclization, oxidation, and crosslinking are listed in Table 4 and were fitted as the peak temperature (T) in the Kissinger equation:

$$-\frac{E_a}{R}=\frac{d\left[ln\left(\frac{\varphi}{T^2}\right)\right]}{d\left(\frac{1}{T}\right)} \quad (1)$$

where E_a is the activation energy (kJ/mol), φ is the heating rate (°C/min), R is the molar gas constant. E_a was taken as the slope of the plots of $\ln(\varphi/T_m^2)$ versus $1/T_m$ in FIGS. **7**G-**7**I and is summarized in Table 5.

TABLE 4

Peak temperatures of cyclization, oxidation, and crosslinking

	15%PAN			0%PAN/10%GNP-3			10%PAN/10%GNP-3		
Rate (°C/min)	T_{Cyc}	T_{Oxi}	T_{Cro}	T_{Cyc}	T_{Oxi}	T_{Cro}	T_{Cyc}	T_{Oxi}	T_{Cro}
1	266.7	167.1	286.5	270.6	164.3	291.9	271.2	166.8	287.4
2.5	281.6	188.4	307.0	283.3	182.4	309.5	284.1	185.9	306.7
5	292.4	205.5	321.3	292.8	204.1	326.8	296.5	205.1	321.1
10	304.6	-	-	307.4	-	-	309.5	-	-
15	312.7	213.8	328.1	314.8	217.3	357.1	317.9	211.5	342.5

TABLE 5

Activation energies determined from the Kissinger method

Activation energy (KJ mol^{-1})	15%PAN	0%PAN/10% GNP-3	10%PAN/10% GNP-3
Cyclization	146.5	151.8	144.5
Oxidation	84.2	77.5	88.4
Crosslinking	138.5	112.1	132.4

[0046] The cyclization activation energies (FIG. **7**G) were not greatly affected by GNP's addition in the middle layer. However, the activation energies for oxidation (FIG. **7**H) and crosslinking (FIG. **7**I) of the 0%PAN/10%GNP-3 fiber showed lower values than the 15%PAN and 1-%PAN/10% GNP-3 fibers. Since oxidation and crosslinking require an oxidative environment to proceed, one possible explanation is due to the faster oxygen diffusion in the middle layer, indicating a void containing structure. As the 0%PAN/10% GNP-3 fiber contained only GNP and DMF in its middle layer, voids were likely to be formed during the solvent exchange process as excess DMF was removed. On the other hand, similar activation energies were observed between the 10%PAN/10%GNP-3 and 15%PAN fibers, indicating a denser structure. DSC shows a coherent result with the cross-sectional SEM images of the 0%PAN10% GNP-3 fiber, indicating a more oxygen permeable structure for low PAN concentration, which could be beneficial to lowering the energy consumption during the stabilization procedure.

[0047] Mechanical analysis. The effect of increasing PAN concentration in the middle layer was analyzed with its mechanical behaviors. As shown in FIG. **8**A, with increasing PAN concentration from 0% to 10%, the mechanical properties showed a significant increase, with modulus increased from 1.2 GPa to 11.07 GPa and ultimate tensile strength increased from 39 MPa to 420 MPa. The weakening of 0%PAN/10%GNP-3 and 5%PAN/10%GNP-3 fibers was primarily caused by the relatively fragile bonding (van der Waals forces) and sliding/exfoliating between graphene or bundles. The stepwise breaking points of the outer and inner layers at the fracture strain of the 0%PAN/10%GNP-3 fiber also suggest weak interfacial interactions between the layers (FIG. **8**A). Furthermore, the aforementioned higher porosity also contributed to higher defects and fractured points under tension.

[0048] FIG. **8**B shows the comparison between various 1% GNP loading fibers with pure PAN fiber. A decrease in both Young's modulus and tensile strength of the D-phase fiber was observed as compared to that of the 15%PAN fiber (Table 6 and FIG. **8**B). It is true that the addition of nanoparticle reinforcement should promote enhanced mechanical properties, but it is also not uncommon to observe a deterioration effect with the inclusion of nanoparticles. Due to the industrial-grade nanoparticle quality and mild sonication dispersion of the GNP, the load transfer at the nanoparticle-polymer interface could be limited for 1 wt% loading. However, under the same nanoparticle dispersing condition, 15% PAN/1%GNP-3 fiber showed a 105% and a 78.9% increase in Young's modulus and ultimate tensile strength, respectively, compared to the D-phase fiber. The enhanced reinforcement efficiency between the D-phase and 3-layer fibers is most likely due to the layered structure through the 3D printed multiphase spinneret. During the fiber spinning procedure, the exterior PAN layer was in close contact with the hot plate, and polymer chains were stretched above the glass transition temperature. The extended polymer chains on the exterior layer and the less extended polymer chains in the interior layer generated shear stress upon the middle layer, which contains graphene materials. This shear stress applied during the thinning process would gradually slide the gra-

phene layers and simultaneously align the graphitic layers more with the fiber axis. However, the exfoliation of graphene layers depends at least in part on the balance between the polymer-nanoparticle interfacial bonding and the amplitude of the graphene interlayer strength. There may be thinner graphene layers when the polymer-nanoparticle bonding is stronger than the van der Waals force between graphene stacks. The thinning and preferential alignment of 2D materials lead to anisotropic electron transport or stress transfer. Thus, high-performance multifunctional fibers are obtained. The content of PAN in the middle layer is expected to serve as a constraint and lubricant to graphene powders, causing thinning/exfoliations of the graphene. As a result, the 2D layer would remain between polymer channels without folding or misaligning, preserving planer alignment and efficient interfacial contacts. Intact, unrolled, and extended graphene in nanocomposites will, in turn, allow examination of both the intrinsic graphene mechanics and the coherent reinforcement efficiency of original 2D materials.

[0049] To further asses the reinforcement effects from GNP alignment and exfoliations, and the assisting influences from PAN, the fibers were heat-treated first at 280° C. for stabilization and then at 1250° C. for carbonization. Afterward, PAN remained crystalline and formed a cyclized ladder polymer structure. Raman spectroscopy was performed on the HT-10%PAN/10%GNP-3 fiber to demonstrate the carbonization efficiency across the fiber with the inclusion of middle GNP containing layer. Two points in the core layer and one point in the outer shell layer were used, and their associated Raman signature peak positions and full-width-at-half-maximums (FWHM) were identical, suggesting negligible differences in carbonization efficiency across layer thickness (FIG. **9**, fitted parameters in Table 7).

TABLE 7

The mathematically fitted peak positions of the Raman spectrum across the diameter of the 10%PAN/10%GNP-3 fibers

	D Line		A Line		G Line	
Position	Peak (cm^{-1})	FWHM (cm^{-1})	Peak (cm^{-1})	FWHM (cm^{-1})	Peak (cm^{-1})	FWHM (cm^{-1})
Position 1	1359.7	207.4	1535.8	97.3	1600.2	68.3
Position 2	1359.5	217.8	1545.7	97.1	1604.1	63
Position 3	1360.8	206.9	1542.5	96	1603.1	63.1

[0050] After carbonization, HT-15%PAN/1%GNP-3 fiber exhibited an increase of ~76% in modulus and ~34% increase in strength compared to HT-15%PAN fiber (Table 6) with stress-strain curves shown in FIG. **10**. The enhanced mechanical properties show the effectiveness of including PAN/GNP in terms of mechanical reinforcement. However, the standard deviations for all carbonized fibers are high and mechanical data are more scattered than those fibers without defects (Table 6). Weibull statistical analysis was used to analyze property-defect relationships. Both the Weibull modulus and strength fitted values are listed in Table 8. Scale parameters (x_o) for both fracture strength and tensile modulus followed the same trend as the mechanical parameters proving the applicability of the Weibull equations. x_o showed an increasing trend from HT-15%PAN fiber to 15%PAN/1%CNT-3 fiber, while the HT-15%PAN/1%GNP-3 fiber showed the highest strengthening effects. However, the inclusion of GNP and CNT decreased the shape parameters (β) in strength, suggesting an increase in defect severity. As compared to the CNT inclusion, PAN polymer chains filled the voids among planar graphene layers more easily than in the CNT networks due to the tube wall curvature. Modulus scale parameters (x_o) showed an equal value from HT-15%PAN fiber to 15%PAN/1%CNT-3 fiber, while the HT-15%PAN/1%GNP-3 fiber showed the highest stiffening effects. β showed an opposite trend to those of the strength value because the stiffness reinforcement is mainly related to the alignment of nanoparticles.

TABLE 6

Mechanical properties before and after carbonization

	Pre-carbonized fibers			Carbonized fibers		
Fiber name	E (GPa)	σ (MPa)	ε (%)	E (GPa)	σ (MPa)	ε (%)
15%PAN	9.3 ± 1.8	280 ± 44	8.1 ± 0.1	42.3 ± 11.4	320 ± 110	1.5 ± 0.5
15%PAN/1 %GNP-D	4.4 ± 0.8	190 ± 47	6.8 ± 6.2			
0%PAN/10 %GNP-3	1.3 ± 0.2	39 ± 5	8.4 ± 0.6			
5%PAN/10 %GNP-3	4.5 ± 0.7	190 ± 26	10.2 ± 1.4			
10%PAN/1 0%GNP-3	11.1± 0.9	420 ± 30	8.2 ± 1.1			
15%PAN/1 %GNP-3	9.0 ± 1.0	340 ± 25	9.4 ± 1.3	74.6 ± 17.6	440 ± 150	1.3 ± 0.6
15%PAN/1 %CNT-3	9.8 ± 1.5	320 ± 41	9.6 ± 1.0	38.9 ± 22.2	290 ± 140	1.1 ± 0.9

TABLE 8

Weibull modulus and strength fitted values

	Weibull analysis			
	Modulus fitting		Strength fitting	
Fiber Name	x_o (GPa)	β	x_o (GPa)	β
HT-15%PAN	47.2	3.6	0.34	4.1
HT-15%PAN/1%GNP-3	84.3	4.4	0.53	3.9
HT-15%PAN/1%CNT-3	47.2	3.1	0.38	2.4

x_o, scale parameter suggesting the intrinsic mechanical values; β, shape parameter implying data reliability

[0051] Polarized Raman spectroscopy. FIG. **11**A shows a cross-sectional SEM image of the 15%PAN/1%GNP-3 fiber with an enlarged section shown in FIG. **11**B indicating the aligned GNP. Polarized Raman spectroscopy was used to assess the orientation of the GNP and CNT. The G-band

intensities of both graphene and carbon nanotubes using polarized Raman spectroscopy with different incident angles have been previously studied to determine their orientations. Both the middle and edge sections of the core GNP-containing layer were chosen as the laser incident spots, as depicted in FIG. **11**C, while ø is the angle between the polarization direction and fiber axis. The optical images show the laser spots at ϕ=0° (FIGS. **11**D and **11**E) and 90° (FIGS. **11**F and **11**G) for the edge and middle sections.

[0052] FIGS. **11**H and **11**I show the corresponding response at both the edge and middle of the fiber. When the laser was focused on the edge of the GNP layer, the intensity of the G-band, 1585 cm^{-1}, is smaller at ø =90° compared to ø= 0°. In comparison, when the laser was focused on the middle of the layer, the peak intensities remained the same regardless of ø angle. Schematics in FIGS. **11**J and **11**K show the deduced GNP orientation. The light arrows indicate the direction of the polarized laser and the dark arrows show the corresponding scattered radiation. The angular dependency for the edge of the fiber suggested that the 2D GNP was aligned in the x-axis and was parallel to the x-z plane. The angular in-dependency for the middle of the fiber suggested that the 2D GNP was parallel to the x-y plane. In sum, the orientation is depicted in FIG. **11**L where GNP nanoparticles were likely to be distributed in a concentric geometry with respect to the layers. This GNP morphology is highly consistent with the generation of shear stress across two different phases during the hot-drawing procedure as previously mentioned.

[0053] As one-dimensional nanoparticles, carbon nanotubes will generate different spectral features from two-dimensional graphene depending on the incident point. FIGS. **11**M and **11**N show the polarized Raman spectra for the 15%PAN/1%CNT-3 fiber at both the edge and the middle sections with FIGS. **12**A and **12**B depicting the orientation of each case. Since intensities of G-band show strong angular dependency at both the edge and the middle of fiber and due to the 1D geometry, CNTs are expected to be aligned in the fiber axial direction.

[0054] Electrical properties for sensor applications. Pure PAN showed resistance beyond the testing capability of a multimeter; upon stabilization and carbonization, these fibers had a measured conductivity of 151.8 S/cm shown in FIG. **13**A. The conductivity is between 12.5-20.0 S/cm for amorphous carbons, 200-300 S/cm for graphitic planes (parallel to the base plane), and 3.3 S/cm for graphitic planes (perpendicular to the base plane). As a comparison to these studies, the HT-15%PAN fibers may have formed continuous carbon pathways for the electrons to flow. The addition of GNP and CNT at a weight percentage of 1 wt% (i.e., 15% PAN/1%GNP-3 and 15%PAN/1%CNT-3, respectively) did not exhibit any noticeable increase in their electrical conductivities before the heat-treatment, mainly due to the reason of not achieving required percolation thresholds. However, there were huge increases in conductivity after carbonization steps (i.e., HT-15%PAN/1%GNP-3 and HT-15%PAN/1%CNT-3, respectively), with the CNT showing a more significant improvement (FIG. **13**A). Experimentally, the intrinsic electrical conductivity can go as high as 10^5 S/cm for a single CNT and 10^6 S/cm for a single layer of graphene. However, theoretically, this electrical conductivity should not vary for graphitic layers, independent of the carbon forms, e.g., carbon nanotubes, graphene, or even graphitic carbon fibers. In practice, it has been found that the number of stacked layers can influence electron flow properties, with the highest deterioration in carbon fibers for the layer stacking or intertwining, and the lowest decrease in carbon nanotubes due to its nanoscale effect. This is consistent with the data presented here that there is a consistently increasing trend in conductivity from carbon fibers to those containing GNP and CNT.

[0055] A chemoresistive sensor based on HT-15%PAN/1%GNP-3 fibers was tested. Three carbon fibers placed in parallel on a rigid substrate were put in a container and tested via an in-house designed sensing setup. A volatile organic compound (VOC) of methanol was chosen for the application as biomarker sensors. According to the Occupational Safety and Health Administration (OSHA), methanol can be harmful to humans at concentrations over 200 ppm over prolonged periods of time. Traditional solid-state VOC sensors often require a relatively high operating temperature due to their semi-conducting nature. The ability to sense these VOCs at room temperature, as the fiber sensor from this study can do, is desired to reduce the operating costs of these sensors. During the sensing tests, methanol vapors with concentrations ranging from 30 ppm, 60 ppm, 120 ppm, and 140 ppm, with a constant total flow of around 300 ml/min, were maintained at room temperature (i.e., 25° C.). Both HT-15%PAN/1%GNP-3 and HT-15%PAN fibers were tested, and their responses were calculated based on $\Delta R/R_0$ where ΔR is the resistance change and R_0 is the initial resistance (FIGS. **13**B and **13**C). With exposure to methanol vapor, an increase of resistance was expected due to the polar nature of methanol that can hinder the movement of charged electrons upon surface absorption. HT-15%PAN/1%GNP-3 fiber showed a much higher response and a much larger signal to noise (SNR) (FIG. **13**D) compared to HT-15%PAN fiber. For 30 ppm concentration, 3-layer fiber showed an SNR of 3.5 while 1-phase fiber showed no distinct signal (SNR=1). This is likely due to the overall higher electrical conductivity induced by the embedded GNP for the 3-layer fiber. Since the surface of the multilayered fiber and pure PAN-based carbonized fiber had the same composition and morphology, the chemoresistive response was expected to be higher for lower R_0 of the HT-15%PAN/1%GNP-3 fiber. The same methanol concentrations were passed through the 3-layer fiber sensor for 5 cycles (FIG. **13**E). The highest concentration (i.e., 140 ppm) showed an average of 8% change in resistance, while the lowest concentration (i.e., 30 ppm) showed an average 0.02% change in baseline resistance.

[0056] The carbonized coaxial composite fiber responds to deformation that can be caused by weight, mechanical compression, or impact encountered in structural health monitoring applications. Thus, the fibers can be used as pressure sensors. FIG. **14**A shows a schematic of the pressure sensor test setup that detects the signal when specific weight or pressure is applied on top of the tested samples. FIGS. **14**B-**14**D show signals collected along path **702** (FIG. **14**B), **704** (FIG. **14**C), and other contacts (FIG. **14**D).

[0057] Particular embodiments of the subject matter have been described. Other embodiments, alterations, and permutations of the described embodiments are within the scope of the following claims as will be apparent to those skilled in the art. While operations are depicted in the drawings or claims in a particular order, this should not be understood as requiring that such operations be performed in the parti-

cular order shown or in sequential order, or that all illustrated operations be performed (some operations may be considered optional), to achieve desirable results.

[0058] Accordingly, the previously described example embodiments do not define or constrain this disclosure. Other changes, substitutions, and alterations are also possible without departing from the spirit and scope of this disclosure.

What is claimed is:

1. A carbonized coaxial composite fiber comprising:
an inner layer comprising carbonized polyacrylonitrile;
a middle layer surrounding the inner layer and comprising carbonized graphene nanomaterials, wherein the graphene nanomaterials comprise graphene nanoplatelets, graphene nanoribbons, graphene nanochips, or any combination thereof; and
an exterior layer surrounding the middle layer comprising carbonized polyacrylonitrile,
wherein the carbonized graphene nanomaterials are aligned along a length of the coaxial composite fiber.

2. The fiber of claim **1**, wherein the middle layer further comprises carbonized polyacrylonitrile.

3. The fiber of claim **2**, wherein the middle layer is formed from a mixture comprising the polyacrylonitrile and the graphene nanomaterials, and a weight ratio of the polyacrylonitrile to the graphene nanomaterials in the mixture is in a range of 1:15 to 15:1.

4. The fiber of claim **3**, wherein the middle layer defines voids between the carbonized graphene nanomaterials.

5. The fiber of claim **1**, wherein the voids are at least partially filled with polyacrylonitrile.

6. The fiber of claim **1**, wherein the inner layer and the outer layer consist of polyacrylonitrile.

7. The fiber of claim **1**, wherein a diameter of the coaxial composite fiber is in a range of about 50 microns to about 500 microns.

8. The fiber of claim **7**, wherein a diameter of the inner layer is in a range of about 20 microns to about 80 microns.

9. The fiber of claim **7**, wherein a thickness of the middle layer is in a range of about 20 microns to about 10 microns.

10. The fiber of claim **7**, wherein a thickness of the outer layer is in a range of about 10 microns to about 50 microns.

11. A method of forming the coaxial composite fiber of claim **1**, the method comprising:
forming a coagulated gel precursor fiber by extruding a multiplicity of solutions through a multiphase spinneret through an air gap and into a solvent, wherein the coagulated gel precursor fiber comprises:
an inner layer comprising polyacrylonitrile;
a middle layer comprising graphene nanomaterials, wherein the graphene nanomaterials comprise graphene nanoplatelets, graphene nanoribbons, graphene nanochips, or any combination thereof; and
an outer layer comprising polyacrylonitrile;
hot drawing the coagulated gel precursor fiber to yield a drawn precursor fiber;
oxidizing the drawn precursor fiber to yield a stabilized fiber; and
carbonizing the stabilized fiber to yield the coaxial composite fiber.

12. The method of claim **11**, wherein the multiplicity of solutions comprises a first solution, a second solution, and a third solution corresponding to the inner layer, the middle layer, and the outer layer, respectively.

13. The method of claim **12**, wherein the first solution and the third solution comprise polyacrylonitrile.

14. The method of claim **13**, wherein the first solution and the third solution are the same.

15. The method of claim **12**, wherein the second solution comprises graphene nanomaterials.

16. The method of claim **15**, wherein the second solution further comprises polyacrylonitrile.

17. The method of claim **16**, wherein a weight ratio of the polyacrylonitrile to the graphene nanomaterials is in a range of 1:15 to 15:1.

18. The method of claim **12**, wherein the first solution, the second solution, and the third solution comprise dimethylformamide.

19. The method of claim **11**, wherein the solvent comprises methanol.

20. The method of claim **11**, wherein hot drawing the coagulated gel precursor fiber comprises heating the coagulated gel precursor fiber above the glass transition temperature of polyacrylonitrile.

* * * * *